COMPRESSIVE MEASUREMENT OF SPREAD SPECTRUM SIGNALS

by

Feng Liu

A Dissertation Submitted to the Faculty of the

DEPARTMENT OF ELECTRICAL AND COMPUTER ENGINEERING

In Partial Fulfillment of the Requirements
For the Degree of

DOCTOR OF PHILOSOPHY

In the Graduate College

THE UNIVERSITY OF ARIZONA

2 0 1 5

THE UNIVERSITY OF ARIZONA
GRADUATE COLLEGE

As members of the Final Examination Committee, we certify that we have read the dissertation prepared by Feng Liu, titled *Compressive Measurement of Spread Spectrum Signals*, and recommend that it be accepted as fulfilling the dissertation requirement for the Degree of Doctor of Philosophy.

Ali Bilgin	12/18/2014 Date
Michael W. Marcellin	12/18/2014 Date
Bane Vasic	12/18/2014 Date

Final approval and acceptance of this dissertation is contingent upon the candidate's submission of the final copies of the dissertation to the Graduate College.

I hereby certify that I have read this dissertation prepared under my direction and recommend that it be accepted as fulfilling the dissertation requirement.

Ali Bilgin Dissertation Director	12/18/2014 Date

STATEMENT BY AUTHOR

This dissertation has been submitted in partial fulfillment of requirements for an advanced degree at the University of Arizona and is deposited in the University Library to be made available to borrowers under the rules of the Library.

SIGNED: Feng Liu

ACKNOWLEDGMENTS

I would like to express my sincere gratitude to my advisor, Dr. Ali Bilgin, for the advice in this research work and for his guidance and support throughout my PhD studies. Thanks are also extended to Dr. Michael W. Marcellin and Dr. Bane Vasic for their participation on the committee and for their helpful comments. My fellow graduate students, Mr. Mahesh Keerthivasan, Mr. Sagar Mandava, Mr. Hsin-Chang Feng, Dr. Yookyung Kim, and Mr. Rajagopalan Sundaresan deserve many thanks for their friendship and help during my graduate studies.

To my family, professors, and friends,
whose help and encouragement
made this possible

TABLE OF CONTENTS

LIST OF FIGURES

LIST OF TABLES

ABSTRACT

Spread Spectrum (SS) techniques are methods used in communication systems where the spectra of the signal is spread over a much wider bandwidth. The large bandwidth of the resulting signals make SS signals difficult to intercept using conventional methods based on Nyquist sampling. Recently, a novel concept called compressive sensing has emerged. Compressive sensing theory suggests that a signal can be reconstructed from much fewer measurements than suggested by the Shannon Nyquist theorem, provided that the signal can be sparsely represented in a dictionary. In this work, motivated by this concept, we study compressive approaches to detect and decode SS signals. We propose compressive detection and decoding systems based both on random measurements (which have been the main focus of the CS literature) as well as designed measurement kernels that exploit prior knowledge of the SS signal. Compressive sensing methods for both Frequency-Hopping Spread Spectrum (FHSS) and Direct Sequence Spread Spectrum (DSSS) systems are proposed.

CHAPTER 1

INTRODUCTION

Spread Spectrum (SS) techniques [1] are methods used in communication systems where the spectra of the signal is spread over a wide bandwidth. SS techniques are particularly attractive for secure communications since spreading of the signal bandwidth makes SS signals difficult to jam or intercept. SS signals are also resistant to narrow band interference and are therefore commonly employed in multi-access communication protocols.

Common SS techniques include Frequency-hopping Spread Spectrum (FHSS), Direct Sequence Spread Spectrum (DSSS), and Time-hopping Spread Spectrum (THSS). The focus of this work will be on the two most common SS techniques, FHSS and DSSS.

FHSS is arguably the most common SS technique. In this technique, the frequency of the carrier is switched rapidly between many frequency channels in a pseudorandom manner as illustrated in Figure 1.1. This pseudorandom sequence of frequency channels are known to a cooperative receiver and, therefore, the transmitter and the receiver can communicate in synchronization. However, it is difficult for a non-cooperative receiver without the knowledge of the pseudorandom channel sequence to capture the signal efficiently. Furthermore, FHSS signals are highly resistant to jamming since an adversary without the knowledge of the pseudorandom channel sequence would need to jam a very large bandwidth to block reception of transmitted signals.

In contrast to FHSS, DSSS techniques spread the spectrum of the signal by modulating the signal with Pseudo-noise (PN) sequences. The resulting signal spectra appears as white and has a much wider bandwidth than the original signal as illustrated in Figure 1.2. DSSS signals are also very resistant to interception

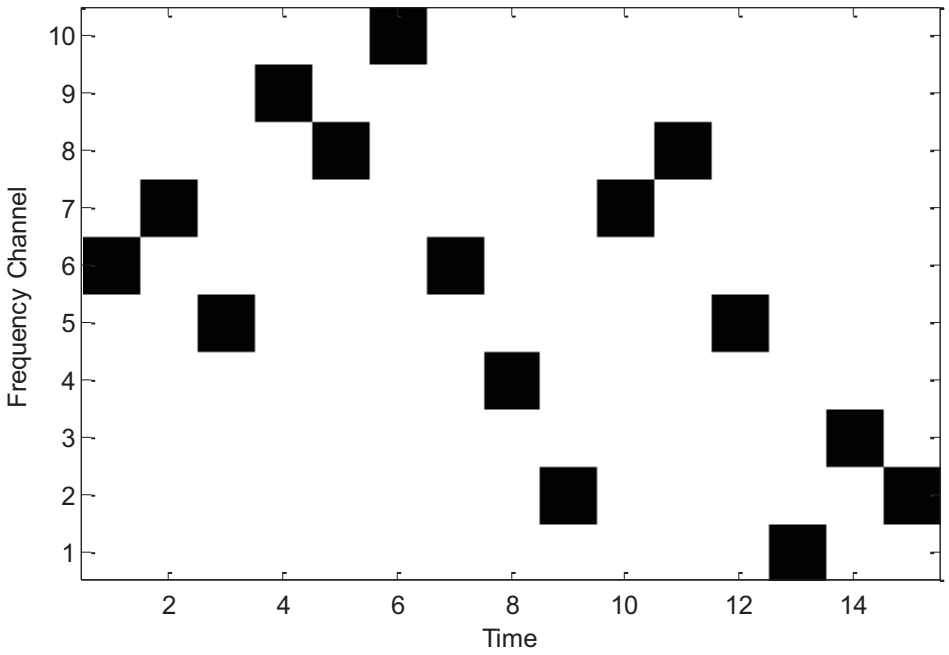

Figure 1.1: Illustration of Frequency-Hopping Spread Spectrum. The dark squares illustrate the frequency channel occupied by the FHSS signal during each time slot.

since the spread signal usually appears as white noise to non-cooperative receivers and is often submerged below the background noise.

Most traditional communication systems are designed based on the celebrated Nyquist-Shannon sampling theorem [2]. Recently, the Compressive Sensing (CS) theory [3, 4] has provided an alternative perspective on sampling. CS theory has shown that signals with sparse representations can be recovered from much fewer measurements than suggested by the Nyquist theory. Since many real-world signals can be represented sparsely, CS theory has attracted significant interest over the last decade. In this dissertation, we study non-cooperative detection and decoding of SS signals based on CS principles. Since the modulated spectra in SS

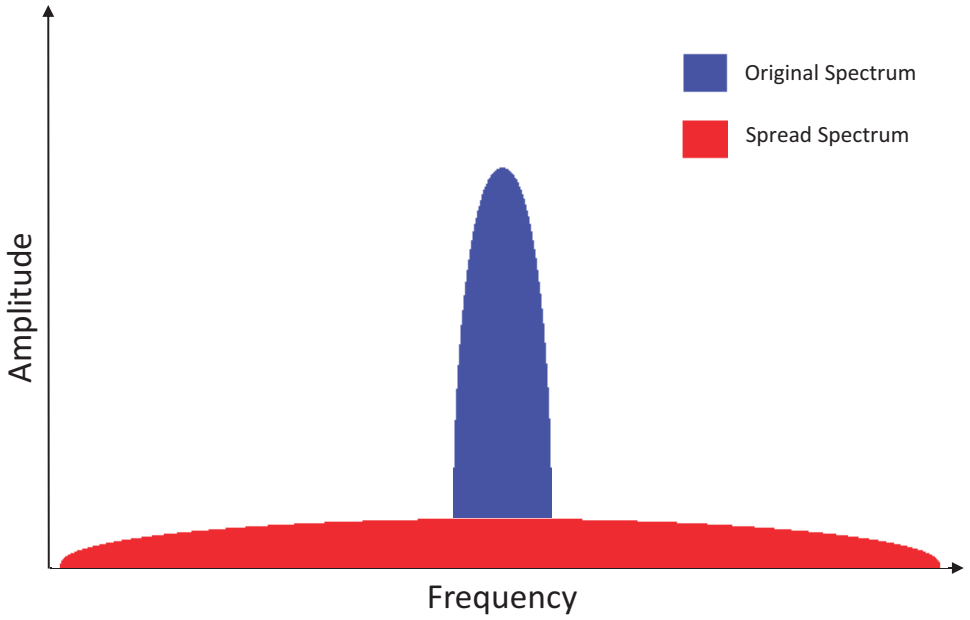

Figure 1.2: Illustration of Direct Sequence Spread Spectrum. The original signal spectrum is spread after modulation with the PN sequence to produce the DSSS signal.

techniques cover a much larger bandwidth than the original signal, capturing this large bandwidth requires conventional Analog-to-Digital Converters (ADCs) to operate at very high sampling rates. These high sampling rates make conventional systems expensive and even impractical. On the other hand, SS signals can be represented sparsely and are amenable to the utilization of CS techniques. Therefore, we present several novel approaches for compressive detection and decoding of SS signals in this dissertation.

1.1 Organization of this Work

The organization of this dissertation is as follows:

In Chapter 2, a brief review of CS theory is provided. The basic CS theory framework including concepts such as sparsity and incoherence are introduced. Chapter 2 also provides an overview of SS techniques. Both FHSS and DSSS methods are reviewed in this chapter.

In Chapter 3, compressive methods for detecting the presence of FHSS signals are proposed. Most of the existing CS literature is based on random compressive measurements. The first method introduced in this chapter also relies on random measurement kernels. Subsequently, two methods that utilize prior information about the structure of FHSS signal to design non-random measurement kernels are introduced. The first method of these methods uses static measurement kernels; the measurement kernels are designed once and utilized throughout the sensing procedure. The second method illustrates how the measurement kernels can be adapted based on information obtained during previous measurement periods. The performance of the proposed methods are compared against conventional methods which use sweeping spectrum analyzers with theoretical analysis and simulations.

In Chapter 4, we introduce compressive methods for detecting the presence of DSSS signals. Conventional detection of DSSS signals is often performed using energy-detection or autocorrelation. Compressive detection approaches for both of these detection strategies are introduced in this chapter. Similar to the compressive detection methods discussed in Chapter 3 for FHSS, detection using random measurement kernels and designed measurement kernels are discussed. The performances of the proposed compressive techniques are compared to conventional methods using theoretical analysis and simulation studies.

The goal of the methods presented in Chapters 3 and 4 is to detect the presence of FHSS and DSSS signals, respectively. Once the presence of spread spectrum signals are confirmed, a natural next-step could be to decode these signals. Therefore,

in Chapter 5, compressive methods for non-cooperative decoding of spread spectrum signals are introduced. The goal of these methods is to recover the symbols from compressive measurements. Similar to previous chapters, both random and designed measurement kernels are proposed. Experimental results are presented to evaluate the performances of the proposed techniques on FHSS and DSSS signals.

Finally, conclusions are drawn and future directions are discussed in Chapter 6.

CHAPTER 2

BACKGROUND

2.1 Compressive Sensing

2.1.1 Concept and Mathematical Framework

Recently, a novel theory called compressive sensing (CS) has emerged [3, 4]. The CS theory states that it is possible to reconstruct a signal from much fewer measurements than suggested by the Nyquist Sampling Theorem [2] if the signal can be sparsely represented based on some dictionary.

The basic sensing problem in CS can be modeled using the linear equation

$$\mathbf{y} = \mathbf{\Phi x} \tag{2.1}$$

where the $N\times1$ vector $\mathbf{x}$ denotes the input signal, the $M\times1$ vector $\mathbf{y}$ denotes the compressive measurement vector, and the $M\times N$ matrix Φ is the matrix representation of the measurement kernel, often referred to as the sensing matrix. The goal of CS is to recover the signal $\mathbf{x}$ from the compressive measurements $\mathbf{y}$ when $M \ll N$.

According to the CS theory, two prerequisites for successful recovery of signals from compressive measurements are sparsity and incoherence. In the following two subsections, we briefly introduce these concepts.

2.1.2 Sparsity

A key tenet of CS theory is that many natural signals have sparse representations. Consider an $N\times1$ vector $\mathbf{x}$. The support of this vector is denoted by $\text{supp}(\mathbf{x}) = \{j : x_j \neq 0\}$. The cardinality of this support is called the ℓ_0-norm of

the vector $\mathbf{x}$ and is denoted by

$$\|\mathbf{x}\|_0 = |\text{supp}(\mathbf{x})| \tag{2.2}$$

A vector $\mathbf{x}$ is called k-sparse if $\|\mathbf{x}\|_0 \leq k$.

The vector $\mathbf{x}$ may not be sparse itself but may have a sparse representation in a dictionary. Let $\mathbf{x}$ be represented as

$$\mathbf{x} = \mathbf{\Psi}\vartheta \tag{2.3}$$

where $\mathbf{\Psi}$ is an $N \times K$ dictionary with each of its columns referred to as the atoms of the dictionary, and ϑ is the $K \times 1$ representation vector. If ϑ is a sparse vector, the signal $\mathbf{x}$ is said to have a sparse representation in dictionary $\mathbf{\Psi}$.

Sparsity of a signal implies that the signal can be represented much more compactly than suggested by its dimension. In fact, many natural signals can be represented sparsely in appropriately chosen dictionaries.

2.1.3 Incoherence

Another key tenet of CS theory is incoherent measurements. The CS theory [5] states that signal $\mathbf{x}$ can be reconstructed from compressively sensed data $\mathbf{y}$ with overwhelming probability, if the number of measurements M satisfies:

$$\mathbf{M} \geq C \cdot \mu^2(\mathbf{\Phi}, \mathbf{\Psi}) \cdot S \cdot \log N \tag{2.4}$$

where C is a positive constant, S is the degree of sparsity of the signal as represented in dictionary $\mathbf{\Psi}$, and

$$\mu(\mathbf{\Phi}, \mathbf{\Psi}) = \sqrt{N} \max_{i,j} |\langle \phi_i, \psi_j \rangle| \tag{2.5}$$

indicates the mutual coherence [6] between the rows of sensing matrix $\mathbf{\Phi}$ (denoted as ϕ_i, with $1 \leq i \leq M$), and the columns of the dictionary $\mathbf{\Psi}$ (denoted as ψ_j, with $1 \leq j \leq K$).

Equation 2.4 suggests that increased incoherence between the sensing matrix and the sparsity dictionary would allow reconstruction of the signal from fewer samples. Decreased incoherence as well as decreased sparsity would require increased number of measurements for successful recovery of the signal.

2.2 Spread Spectrum Signals

2.2.1 Frequency-Hopping Spread Spectrum

Often attributed to multiple inventors in the early part of the twentieth century, FHSS is a common transmission method where the frequency of the carrier is rapidly switched between many frequency channels in a pseudorandom manner. The pseudorandom sequence is known to a cooperative transmitter and receiver pair which allows them to synchronously switch between communication channels. However, pseudorandom switching of the carrier frequency makes FHSS signals difficult to jam and intercept.

There are many different kinds of FHSS signals. In this work, we will focus on Gaussian-Filtered Frequency-Shift Keying (GFSK) modulated FHSS signal as defined by the Bluetooth standard [7] which is a wireless communication standard for transmitting data over short distances.

In the Bluetooth standard, the transmitted symbols are divided into packets. Each packet is transmitted using one of 79 frequency channels. The frequency channels are distributed between 2.402 GHz to 2.480 GHz in 1 MHz steps. A packet consists of 625 symbols and the standard specifies the symbol period to be 1 μs. During each hop, one of the 79 channels is selected randomly using a uniform distribution and one packet is transmitted. Therefore, the hopping period is 625 μs.

The complex FHSS signal during one hop period can be modeled as

$$s(t) = \sqrt{\frac{2E_b}{T}} e^{j(f(t)+\theta)} \tag{2.6}$$

where E_b is the signal energy per symbol, T is the symbol duration, and θ is a constant but unknown phase. $f(t)$ in Equation (2.6) is defined as

$$f(t) = 2\pi f_c t + 2\pi h \sum_{k=0}^{N_s-1} a_k q(t - kT), 0 \leq t \leq N_s T \tag{2.7}$$

where f_c is the frequency of the subcarrier during the current hop period, h is the modulation index, $a_k \in \{+1, -1\}$ is the binary symbol sequence, N_s is the number of symbols transmitted during each hop, and $q(t)$ is the phase pulse defined as

$$q(t) = \int_0^t g(\tau) d\tau \tag{2.8}$$

where $g(t)$ is a Gaussian filter used to smooth frequency transitions between symbol periods. The Gaussian filter $g(t)$ is given by

$$g(t) = \frac{1}{\sqrt{2\pi\sigma^2}} e^{-\frac{1}{2}(\frac{t}{\sigma})^2} \tag{2.9}$$

where $\sigma = \frac{\sqrt{\ln(2)}}{2\pi B_g}$ is a parameter that determines the filter's 3-dB bandwidth B_g. It is important to note that the use of this Gaussian filter results in *Inter-symbol Interference* (ISI). ISI is defined as the distortion in the signal due to one or more symbols interfering with other symbols. The use of the Gaussian filter results in the symbol waveform during one symbol period to interfere with the FHSS signal during other symbol periods.

2.2.2 Direct Sequence Spread Spectrum Signals

Paul Kotowski and Kurt Dannehl at Telefunken are credited for the invention of DSSS in their 1940 patent where they described an encryption device which combines broadband noise with the payload signal [8, 9]. The DSSS technology continues to enjoy widespread adoption today and is used in numerous military and civilian applications. Some example applications include the Direct-Sequence Code Division Multiple Access (DS-CDMA), which is a channel access method in

many mobile phone standards, and the IEEE wireless communications standards 802.11-1999 [10], IEEE 802.11b [11], and 802.11g [12].

In contrast to FHSS, the carrier frequency of DSSS signals stay at a fixed frequency during transmission. The narrowband input signal is spread by modulating the signal with a pseudorandom chip sequence. Such modulation causes the resulting signal spectra to be much wider in bandwidth than the spectra of the original signal. A co-operative receiver with knowledge of the spreading sequence can recover the original narrowband signal by de-spreading. However, detecting the presence of or decoding a DSSS signal without the knowledge of the spreading sequence are difficult tasks since the DSSS signals are often below background noise levels after spreading. In addition, DSSS signals are very resistant to narrowband interference or jamming. A narrowband jamming signal is spread over a large bandwidth during the de-spreading process and the impact of the jamming signal is greatly reduced.

The spreading sequences used in DSSS systems are random bit streams known only to co-opereative transmitter and receiver pairs. Therefore, it is desired that these PN sequences are random and unpredictable. In practice, PN sequences are generated using pseudorandom number generators. The PN generators are often feedback shift registers implemented in hardware as shown in Figure 2.1. In the figure, $C_0, C_1, \cdots, C_{n-1} \in \{0, 1\}$ denote coefficients and $S_0, S_1, \cdots, S_{n-1} \in \{0, 1\}$ denote the contents of the registers. The sum operations are binary sums and the register contents are initialized with a seed. Given the initial seed, these feedback shift registers generate sequences that appear to be random. Figure 2.1 also illustrates a converter added to the end of the feedback shift register to convert the 0/1 values to -1/1 values.

One of the most common types of PN sequences generated using these feedback shift registers are the maximum-length sequences (m-sequences) [13]. These sequences are referred to as "maximum-length" because the output sequence will cycle through every binary sequence (except the zero vector) that can be repre-

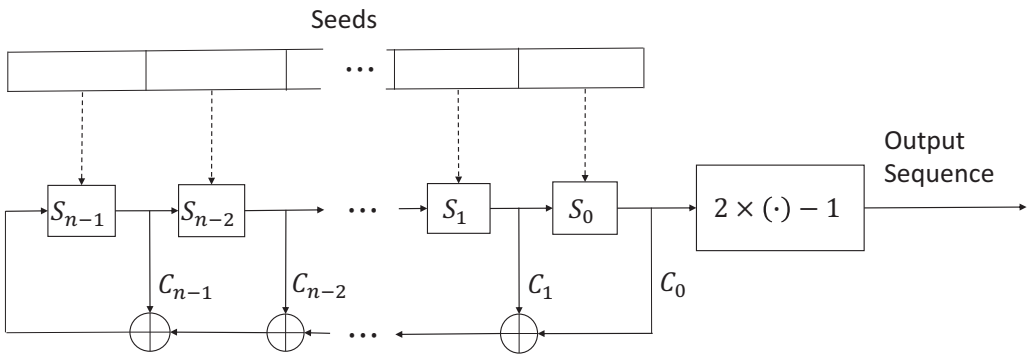

Figure 2.1: Feedback Shift Register for PN sequence generation.

sented by the feedback shift register before repeating. To generate m-sequences, the register coefficients are chosen from primitive polynomials, denoted as $1 + C_{n-1}x + C_{n-2}x^2 + \cdots + C_1x^{n-1} + C_0x^n$. All the primitive polynomials with the orders ranging from 1 to 5 are shown in Table 2.1. The length of m-sequences with the order n is $2^n - 1$, which is equal to the number of valid (i.e. non-zero) seeds.

M-sequences have many additional desirable properties: They are simple to implement in hardware and software, and feedback shift registers with relatively low-orders can generate long sequences. They are also balanced in the sense that the occurrences of 0s and 1s in the sequence are approximately equal. The auto-correlation function of an m-sequence is very close to a train of delta functions.

DSSS techniques are classified into Short-code (SC) and Long-code (LC) DSSS depending on the length of the symbol period. In SC DSSS, the symbol period is the same as the PN sequence period whereas in LC DSSS, the symbol period is shorter than the PN sequence period.

In this work, we focus on SC Binary Phase-Shift-Keying (BPSK) DSSS sig-

Order	Primitive Polynomials	Number of Possible Sequences (Number of Seeds × Number of Polynomials)
1	$1+x$	$1\times1=1$
2	$1+x+x^2$	$3\times1=3$
3	$1+x+x^3$ $1+x^2+x^3$	$7\times2=14$
4	$1+x+x^4$ $1+x^3+x^4$	$15\times2=30$
5	$1+x^2+x^5$ $1+x+x^2+x^3+x^5$ $1+x^3+x^5$ $1+x+x^3+x^4+x^5$ $1+x^2+x^3+x^4+x^5$ $1+x+x^2+x^4+x^5$	$31\times6=186$

Table 2.1: Primitive Polynomials with Orders Ranging from 1 to 5

nals generated using m-sequences as representative DSSS signals. With known synchronization and phase, BPSK DSSS signals can be modeled as

$$s(t) = A \sum_{l=-\infty}^{\infty} d_l \sum_{k=0}^{N-1} c_k v(t - lT_s - kT_c) \tag{2.10}$$

where A denotes the magnitude of the DSSS signal; $d_l \in \{-1, 1\}$ denotes the l^{th} entry of the symbol sequence; $c_k \in \{-1, 1\}$ for $0 \leq k \leq N-1$ denotes the $(k+1)^{th}$ entry of the PN sequence with the length N; $v(t)$ is a rectangular function with the width of chip period T_c; and T_s is the symbol period. In our subsequent analysis, we consider all m-sequences of orders 1 to 5 as possible PN sequences. We fix the symbol periods and vary the chip periods in order to vary the m-sequence order. When we refer to the Nyquist sampling rate of DSSS modulated signals, we refer to the Nyquist sampling rate corresponding to the largest spread bandwidth among

the possible signals.

CHAPTER 3

COMPRESSIVE DETECTION OF FREQUENCY-HOPPING SPREAD SPECTRUM SIGNALS

In this chapter, we introduce non-cooperative compressive detection methods to detect the presence of FHSS signals. The chapter starts with an introduction to the presence detection problem and a review of existing methods. The first compressive detection approach introduced in this chapter uses random measurements. Next, two additional detection methods, which illustrate how prior information about the FHSS signal can be incorporated into measurement kernel design, are proposed. Results are provided to compare the proposed approaches with conventional methods and conclusions are drawn at the end of the chapter.

3.1 Introduction

As discussed in Section 2.2.1, FHSS signals hop between frequency channels to avoid interference and detection. This added ambiguity makes their detection difficult. The increased complexity of this detection problem has motivated many methods of detection and interception. While many novel methods (e.g. wavelet based detection [14–19], likelihood based detection [20–25], time-frequency feature analysis based detection [14, 26–30]) have been proposed, conventional approaches can be broadly classified into energy based and autocorrelation based detection methods [26]. Autocorrelation based methods [19, 31–33] are often non-linear and more difficult to implement so energy based detection approaches [34–43] are often preferred in practice. Furthermore, our proposed compressive detection approaches are also based on energy detection so we concentrate on conventional energy based detection approaches in this section.

Among conventional FHSS detection approaches, the most common method is to use channelized radiometers. A typical radiometer uses a bandpass filter to select the frequency band over which measurements are made. Since FHSS signals hop over large frequency ranges, energy measurements are needed over large bandwidths. A common method to measure energy over a large frequency range is to use a Sweeping Spectrum Analyzer (SSA) [24, 37, 38, 44, 45]. The block diagram of a typical SSA is shown in Figure 3.1. Here, the input signal is mixed with the signal from a Voltage Controlled Oscillator (VCO). The mixed signal is passed through a low-pass filter and the filter output is sampled. The samples are used to detect the presence or absence of FHSS signals. By sweeping the frequency of the VCO signal, SSA scans different frequency ranges.

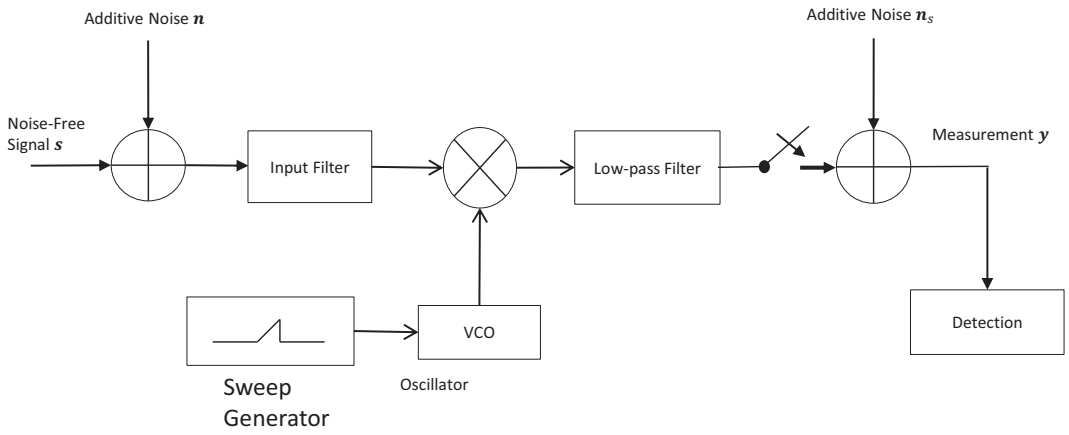

Figure 3.1: Scanning Spectrum Analyzer

Let B denote the full frequency hopping range of the FHSS signal. Let's also assume that the SSA uniformly divides this range into N_b subbands which are scanned sequentially. Then, the Nyquist sampling rate used to scan each subband is computed with respect to the bandwidth of each subband B/N_b. Let α denote

the relative scanning rate which is defined as the number of scanning intervals per FHSS hopping period. Note that when $\alpha \geq N_b$, SSA scans the entire hopping frequency range before the signal hops. We refer to this regime as the *fast scanning regime*. Conversely, when $\alpha < N_b$, the signal hops before the SSA scans the entire hopping frequency range. We refer to this regime as the *fast hopping regime*. To simplify our analysis, we assume that α is either a rational number of 1 divided by a positive integer or a positive integer that can divide or be divided by N_b.

During the i^{th} scanning interval, the relationship between the measurement vector $\mathbf{y}_i$ and the FHSS signal $\mathbf{s}_i$ can be modeled by

$$\mathbf{y}_i = \mathbf{\Phi}_i(\mathbf{s}_i + \mathbf{n}_i) + \mathbf{n}_{s_i} \tag{3.1}$$

where $\mathbf{n}_i$ denotes the additive channel noise, $\mathbf{n}_{s_i}$ denotes the quantization noise, and $\mathbf{\Phi}_i$ denotes the matrix representation of the measurement kernel during the i^{th} scanning interval. Here, measurements are obtained by applying a bandpass filter to the noisy input signal so the matrix $\mathbf{\Phi}_i$ represents this bandpass filtering process. In this discretized notation, if the signal $\mathbf{s}_i$ is discretized at the Nyquist rate corresponding to the full hopping bandwidth to yield N samples and M measurements are made during the i^{th} scanning interval, the matrix $\mathbf{\Phi}_i$ will have the dimensions $M \times N$. Since the effect of the quantization noise $\mathbf{n}_{s_i}$ is often much smaller than that of the channel noise $\mathbf{n}_i$, we will ignore $\mathbf{n}_{s_i}$ in our subsequent analysis. $\mathbf{n}_i$ is modeled as zero-mean additive white Gaussian noise with variance σ_n^2 covering the entire FHSS hopping range. To simply our derivations, $\mathbf{s}_i$ is also modeled as a zero-mean Gaussian white signal with variance σ_s^2 within the scanning support that it falls in.

During each scanning period, the decision on the presence or absence of the FHSS signal can be made based on energy detection. This detection problem can be formulated as a choice between two hypotheses:

$$H_0 : \mathbf{y}_i = \mathbf{\Phi}_i \mathbf{n}_i \tag{3.2}$$

$$H_1 : \mathbf{y}_i = \mathbf{\Phi}_i(\mathbf{s}_i + \mathbf{n}_i) \tag{3.3}$$

where H_0 and H_1 denote the signal absent and signal present hypotheses in the i^{th} scanning interval, respectively. Given the detection decisions made in each scanning interval, the final detection decision is made after the entire FHSS hopping range is observed. If the decision "signal present" is made in at least one of the scanning intervals, the final decision "signal present" is made; otherwise, the final decision "signal absent" is made.

Let λ_i denote the measurement energy during the i^{th} scanning interval. When the signal is absent, the distribution of λ_i is given by:

$$pr(\lambda_i|\text{signal absent in } i\text{th scan}) = \frac{{\lambda_i}^{(M-1)} e^{-\frac{\lambda_i}{{\sigma_n}^2}}}{{\sigma_n}^{2M}\Gamma(M)} \tag{3.4}$$

where M denotes the number of measurements during each scanning interval and $\Gamma(\cdot)$ denotes the gamma function. It should also be noted that this distribution was obtained assuming that the filters used in SSA are ideal filters. Using the distribution in Equation (3.4), the theoretical false positive rate (FPR) during the i^{th} scanning interval is calculated by

$$FPR_i = \int_{T_i}^{+\infty} pr(\lambda_i|\text{signal absent in } i\text{th scan})d\lambda_i \tag{3.5}$$

where T_i denotes the detection threshold used during the i^{th} scanning interval. The overall theoretical FPR (i.e. the FPR associated with the final detection decision after all N_B subbands are scanned) is then calculated by:

$$FPR = 1 - \prod_{i=1}^{N_b}(1 - FPR_i) \tag{3.6}$$

When the signal is present, the overall false negative rate depends on the relative scanning rate α. If the scanning rate is not faster than the FHSS hopping rate (i.e., $\alpha \leq 1$), the scanning intervals are independent. The distribution of the measurement energy during the i^{th} scanning interval is then calculated as:

$$pr(\lambda_i|\text{signal present in } i\text{th scan}) = \sum_{k=0}^{\frac{1}{\alpha}} \binom{\frac{1}{\alpha}}{k} (p_i)^k (1-p_i)^{\frac{1}{\alpha}-k} \frac{{\lambda_i}^{(M-1)} e^{-\frac{\lambda_i}{\alpha k N_b {\sigma_s}^2 + {\sigma_n}^2}}}{(\alpha k N_b {\sigma_s}^2 + {\sigma_n}^2)^M \Gamma(M)} \tag{3.7}$$

where p_i denotes the probability that the i^{th} subband is occupied by the FHSS signal at any given time. Using this distribution, the theoretical true positive rate (TPR) during the i^{th} scanning interval is given by

$$TPR_i = \int_{T_i}^{+\infty} pr(\lambda_i|\text{signal present in } i\text{th scan})d\lambda_i \tag{3.8}$$

The overall theoretical TPR (i.e. the TPR associated with the final detection decision after all N_B subbands are scanned) is then given by:

$$TPR = 1 - \prod_{i=1}^{N_b}(1 - TPR_i) \tag{3.9}$$

We consider the case when $1 < \alpha < N_b$ next. In this case, the scanning rate is fast enough to cover multiple subbands during a single hopping period. More specifically, the SSA can scan α subbands before the signal hops. We can therefore consider that the entire set of N_b subbands are divided into $\frac{N_b}{\alpha}$ groups with α subbands each. We refer to these as *scan groups*. The FNR during the j^{th} scan group (containing the $((j-1)\alpha+1)^{th}$ to the $j\alpha^{th}$ scanning interval) is calculated by:

$$FNR_{g,j} = \sum_{i=(j-1)\alpha+1}^{j\alpha} p_i FNR_{gp,ij} + [1 - \sum_{i=(j-1)\alpha+1}^{j\alpha} p_i]FNR_{ga,j} \tag{3.10}$$

where $FNR_{gp,ij}$ denotes the FNR when the signal falls into the support of the i^{th} scanning interval during the j^{th} scan group and $FNR_{ga,j}$ denotes the FNR when the signal is out of the support of the j^{th} scan group during the j^{th} scan group. $FNR_{gp,ij}$ and $FNR_{ga,j}$ can be calculated, respectively, as:

$$FNR_{gp,ij} = \int_{-\infty}^{T_i} \frac{{\lambda_i}^{(M-1)} e^{-\frac{\lambda_i}{N_b{\sigma_s}^2+{\sigma_n}^2}}}{(N_b{\sigma_s}^2+{\sigma_n}^2)^M \Gamma(M)} d\lambda_i \cdot \prod_{\substack{k=(j-1)\alpha+1 \\ k\neq i}}^{j\alpha} \int_{-\infty}^{T_k} \frac{{\lambda_k}^{(M-1)} e^{-\frac{\lambda_k}{{\sigma_n}^2}}}{{\sigma_n}^{2M}\Gamma(M)} d\lambda_k \tag{3.11}$$

and

$$FNR_{ga,j} = \prod_{i=(j-1)\alpha+1}^{j\alpha} \int_{-\infty}^{T_i} \frac{{\lambda_i}^{(M-1)} e^{-\frac{\lambda_i}{{\sigma_n}^2}}}{{\sigma_n}^{2M}\Gamma(M)} d\lambda_i \tag{3.12}$$

The overall theoretical TPR (after all scan groups have been scanned) for this case is given by

$$TPR = 1 - \prod_{j=1}^{\frac{N_b}{\alpha}} FNR_{g,j} \tag{3.13}$$

Finally, we consider the case when the scanning rate is much faster than the hopping rate such that the scanner can scan all N_b subbands before the signal hops. In this case, $\alpha \geq N_b$. It is easy to see that this case can be considered as having a single scan group which contains all subbands. Therefore, the FNR when the signal falls into the support of the i^{th} scanning interval during the single scan group, denoted as $FNR_{gp,i}$, in this case can be obtained by:

$$FNR_{gp,i} = \int_{-\infty}^{T_i} \frac{{\lambda_i}^{(M-1)} e^{-\frac{\lambda_i}{N_b {\sigma_s}^2 + {\sigma_n}^2}}}{(N_b {\sigma_s}^2 + {\sigma_n}^2)^M \Gamma(M)} d\lambda_i \cdot \prod_{\substack{k=1 \\ k \neq i}}^{N_b} \int_{-\infty}^{T_k} \frac{{\lambda_k}^{(M-1)} e^{-\frac{\lambda_k}{{\sigma_n}^2}}}{{\sigma_n}^{2M} \Gamma(M)} d\lambda_k \tag{3.14}$$

Then, the TPR is calculated by:

$$TPR = 1 - \sum_{i=1}^{N_b} p_i FNR_{gp,i} \tag{3.15}$$

The false negative and true positive rates calculated above can be used to evaluate the detection performance of SSAs. As we will illustrate in Section 3.4, SSAs suffer from a "floor" problem in their FNR when $\alpha < N_b$. This floor is due to the non-zero probability that the SSA will miss the hopping signal if the scan rate of the SSA is not fast enough to cover the entire hopping range before the signal hops. A detailed evaluation of this floor problem is presented in Section 3.4.

3.2 Compressive Detection of Frequency-Hopping Spectrum Signals

As discussed in Section 2.1, the recent CS theory provides a novel perspective on sufficient sampling. CS theory illustrates that signals that are sparse in some

domain can be recovered from a small number of linear incoherent measurements. Motivated by this recent result and the fact that FHSS signals are instantaneously sparse in frequency domain, we investigate compressive approaches to detect the presence of FHSS signals. It is worth pointing out that the CS theory, as presented in the seminal works of Candes et. al [3] and Donoho [4], discusses a signal recovery problem. In contrast, we consider a signal detection problem in this work. Furthermore, majority of the literature on CS relies on random measurements. While we investigate the use of random measurements in this work, we also illustrate that measurement kernels designed by incorporating prior information about the underlying signal can yield enhanced performance.

We start this section by introducing our compressive detection framework. The block diagram of the proposed framework is shown in Figure 3.2. In this architecture, the noisy input signal is mixed with wide-band measurement kernels and passed through a low-pass filter (i.e. integrator). The output of the low-pass filter is sampled at a rate much lower than the one suggested by the Nyquist Sampling Theorem. Therefore, this measurement system is compressive. The compressive measurements are then used to detect the presence or absence of FHSS signals. It is worth pointing out that this architecture is very similar to the SSA architecture shown in Figure 3.1 with the exception that the measurements are obtained using wide-band measurement kernels in this case whereas the SSA uses band-limited measurement kernels.

In this framework, the relationship between the measurement vector $\mathbf{y}$ and the signal $\mathbf{s}$ can be modeled by

$$\mathbf{y} = \mathbf{\Phi}(\mathbf{s} + \mathbf{n}) + \mathbf{n_s} \tag{3.16}$$

where $\mathbf{n}$ denotes the additive white Gaussian channel noise with zero-mean and variance σ_n^2 over the entire spread spectrum range. Similar to Equation 3.1, $\mathbf{n}_s$ denotes the quantization noise which we ignore in our analysis since the effect of the quantization noise $\mathbf{n}_s$ is often much smaller than that of the channel noise $\mathbf{n}$.

In our analysis, we divide the measurement process into N_b sequential obser-

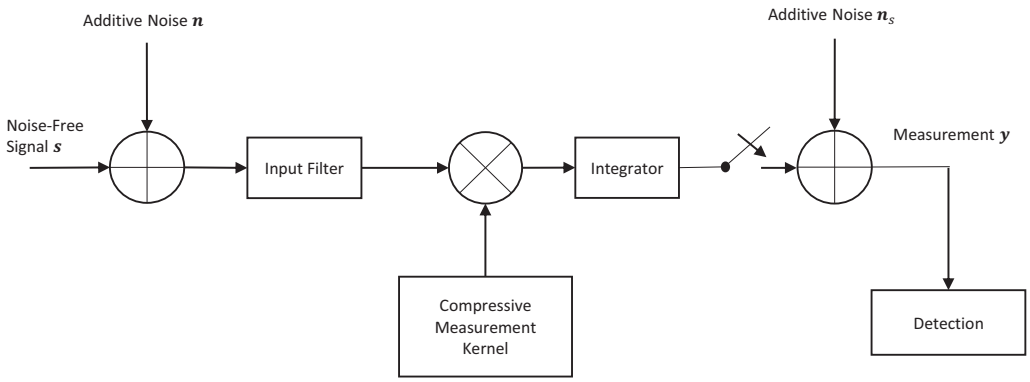

Figure 3.2: Compressive Detector

vation intervals. During each observation interval i, the measurements, the signal, and the channel noise are denoted by $\mathbf{y}_i$, $\mathbf{s}_i$ and $\mathbf{n}_i$ respectively. Naturally, by concatenating $\mathbf{y}_i$ for $1{\leq}i{\leq}N_b$, the full measurement vector $\mathbf{y}$ can be obtained. Similarly, the signal vector $\mathbf{s}$ and the noise vector $\mathbf{n}$ can be obtained by concatenating vectors $\mathbf{s}_i$ and $\mathbf{n}_i$, respectively, for $1{\leq}i{\leq}N_b$. During each observation interval, the $M{\times}N$ measurement kernel is denoted by $\mathbf{\Phi}_i$. The full measurement matrix $\mathbf{\Phi}$ is a $MN_b{\times}NN_b$ block-diagonal matrix where the diagonal blocks consist of $\mathbf{\Phi}_i$ for $1{\leq}i{\leq}N_b$.

The detection problem can be formulated as a decision between two hypothesis:

$$H_0 : \mathbf{y} = \mathbf{\Phi}\mathbf{n} \tag{3.17}$$

$$H_1 : \mathbf{y} = \mathbf{\Phi}(\mathbf{s} + \mathbf{n}) \tag{3.18}$$

where H_0 and H_1 denote the signal absent and signal present hypotheses, respectively.

To counter the correlations introduced by the arbitrary measurement kernels $\mathbf{\Phi}_i$

during each observation interval, a pre-whitening step is used. The measurement during each observation interval, $\mathbf{y}_i$, is pre-whitened using

$$\widetilde{\mathbf{y}}_i = \mathbf{S}_i{}^{+}\mathbf{V}_i{}^{\dagger}\mathbf{y}_i \tag{3.19}$$

where $^{+}$ denotes pseudoinverse; † denotes conjugate transpose; and the matrices $\mathbf{S}_i$ and $\mathbf{V}_i$ are obtained using the singular value decomposition of the measurement kernel matrix during the i^{th} observation interval, $\mathbf{\Phi}_i$:

$$\mathbf{\Phi}_i = \mathbf{V}_i\mathbf{S}_i\mathbf{U}_i{}^{\dagger} \tag{3.20}$$

The final decision is made by thresholding the energy of $\widetilde{\mathbf{y}}$ which is obtained by concatenating $\widetilde{\mathbf{y}}_i$ for $1 \leq i \leq N_b$.

Since we are interested in compressive measurements, it is worth defining the Compression Ratio (CR) in this setting. Given that N is the number of samples needed to sample the signal at the Nyquist rate and M is the number of measurements, the compression ratio is given by $CR = \frac{N}{M}$. For measurement system shown in Figure 3.2, the measurement matrix in each observation interval, $\mathbf{\Phi}_i$, is block-diagonal with each block to be a $1 \times CR$ vector. As an example, a measurement matrix $\mathbf{\Phi}_i$ with $N = 320$ and $M = 16$ (which corresponds to $CR = 20$) is illustrated in Figure 3.3. In the figure, the zero elements of the matrix are shown in black and the non-zero entries are shown in white. The block diagonal structure of the matrix is evident in the figure.

3.2.1 Random Measurement Kernels

As discussed earlier, most of the existing CS methods rely on random measurement kernels since random measurement kernels yield, with high probability, incoherent measurements with any sparsity dictionary. In our compressive detection framework, random measurements can be obtained by randomly selecting the non-zero entries of the measurement matrix $\mathbf{\Phi}$. Let λ denote the energy of the pre-whitened measurements $\widetilde{\mathbf{y}}$. In this case, we model the input FHSS signal $\mathbf{s}$ as

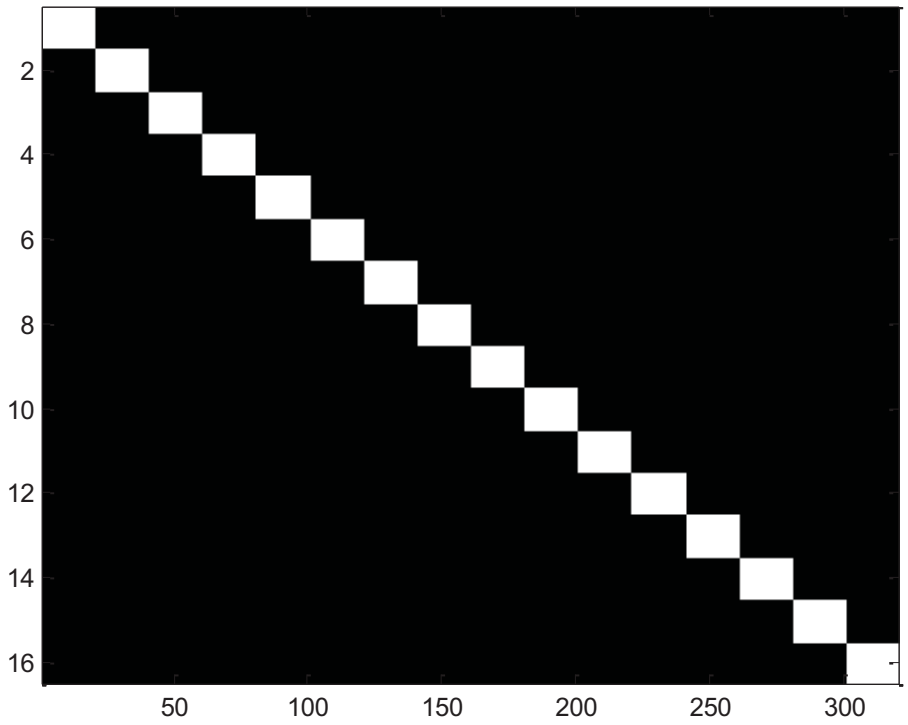

Figure 3.3: Form of a 16×320 Dimensional Sensing Matrix

a zero-mean Gaussian white signal with the variance σ_s^2 over the spread spectrum. The distribution of λ for the signal absent case is then given by:

$$pr(\lambda|\text{signal absent}) = \frac{\lambda^{(R-1)} e^{-\frac{\lambda}{\sigma_n{}^2}}}{\sigma_n{}^{2R}\Gamma(R)} \tag{3.21}$$

where R is the rank of the measurement matrix $\mathbf{\Phi}$. When the non-zero entries of the measurement matrix $\mathbf{\Phi}$ are selected at random, $R = MN_b$ with high probability.

For the signal present case, the distribution of the measurement energy λ is given by:

$$pr(\lambda|\text{signal present}) = \frac{\lambda^{(R-1)} e^{-\frac{\lambda}{(\sigma_s{}^2+\sigma_n{}^2)}}}{(\sigma_s{}^2 + \sigma_n{}^2)^R\Gamma(R)} \tag{3.22}$$

Similar to the SSA case, signal detection can be performed by energy thresholding. Given a threshold T, the theoretical false positive rate of this compressive

detection system is calculated by:

$$FPR = \int_{T}^{+\infty} pr(\lambda|\text{signal absent})d\lambda \tag{3.23}$$

and the theoretical false negative rate is calculated by:

$$FNR = \int_{-\infty}^{T} pr(\lambda|\text{signal present})d\lambda \tag{3.24}$$

From Equations 3.23 and 3.24, we can see that the detection performance of our proposed compressive detection system does not depend on the relative measurement rate, α. This is an important advantage of the proposed compressive detection system over the SSA based detection systems. Results in Section 3.4 will quantify this advantage.

3.3 Knowledge Enhanced Compressive Detection of Frequency-Hopping Spread Spectrum Signals

While most of the CS literature relies on random measurement kernels, there is existing work [46, 47] which illustrates that measurement kernels designed using prior knowledge of the signal and the measurement system can improve performance. In particular, task-specific optimal design of compressive systems based on an information-theoretic metric called Task Specific Information (TSI) was introduced in [46, 47]. The TSI is defined as the mutual information between the virtual source variable and the measurements. The basic principle in this novel sensing framework is to encode the task as a random variable (referred to as the virtual source variable) and to design the measurement kernels to maximize the mutual information between the virtual source variable and the measurements.

The virtual source variable in the TSI framework can be defined for the given task. In our work, we define TSI as the mutual information between the FHSS signal and the measurements as shown in Figure 3.4. Instead of using random measurement kernels, our goal is to design measurement kernels that will maximize

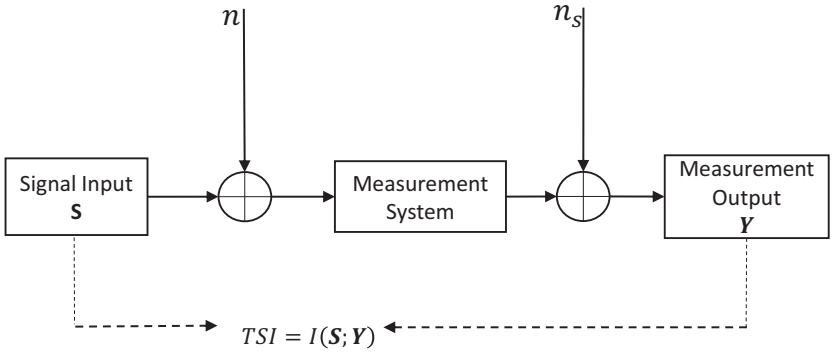

Figure 3.4: Definition of Task Specific Information

TSI. Specifically, considering the block-diagonal structure with single rows as its blocks in the measurement matrix in each observation interval, during an arbitrary i^{th} observation interval, we obtain the m^{th} block of the measurement matrix $\mathbf{\Phi}_i$ (which we denote by $\mathbf{\Phi}_{i,m}$) such that:

$$\mathbf{\Phi}_{i,m} = \arg\max_{\hat{\mathbf{\Phi}}_{i,m}} I(\mathbf{y}_{i,m}; \mathbf{s}_{i,m}),\ s.t.\ \mathbf{y}_{i,m} = \hat{\mathbf{\Phi}}_{i,m}(\mathbf{s}_{i,m} + \mathbf{n}_{i,m}) \tag{3.25}$$

where $\mathbf{s}_{i,m}$, $\mathbf{n}_{i,m}$ and $\mathbf{y}_{i,m}$ denote the signal, the noise, and the measurements, respectively. In order to solve Equation 3.25, an iterative gradient method is implemented. At each iteration, $\mathbf{\Phi}_{i,m}$ is refined using

$$\mathbf{\Phi}_{i,m}^{(j+1)} = \mathbf{\Phi}_{i,m}^{(j)} + \mu \nabla_{\mathbf{\Phi}_{i,m}} I(\mathbf{y}_{i,m}; \mathbf{s}_{i,m}) \tag{3.26}$$

where $\mathbf{\Phi}_{i,m}^{(j)}$ and $\mathbf{\Phi}_{i,m}^{(j+1)}$ denote the m^{th} block of $\mathbf{\Phi}_i$ after j and $j+1$ iterations, respectively, and μ denotes the step size.

The TSI metric in Equation 3.25 can be expanded as:

$$I(\mathbf{y}_{i,m}; \mathbf{s}_{i,m}) = H(\mathbf{y}_{i,m}) - H(\mathbf{y}_{i,m}|\mathbf{s}_{i,m}) \tag{3.27}$$

We note that the term $H(\mathbf{y}_{i,m}|\mathbf{s}_{i,m})$ only depends on noise power and has no effect on the maximization problem of Equation 3.25 for a given noise level. Therefore, equivalent forms of Equations 3.25 and 3.26 can be given, respectively, as:

$$\mathbf{\Phi}_{i,m} = \arg\max_{\hat{\mathbf{\Phi}}_{i,m}} H(\mathbf{y}_{i,m}),\ s.t.\ \mathbf{y}_{i,m} = \hat{\mathbf{\Phi}}_{i,m}\mathbf{s}_{i,m} \tag{3.28}$$

and

$$\mathbf{\Phi}_{i,m}^{(j+1)} = \mathbf{\Phi}_{i,m}^{(j)} + \mu\nabla_{\mathbf{\Phi}_{i,m}} H(\mathbf{y}_{i,m}) \tag{3.29}$$

The problems represented by Equations 3.28 and 3.29 can be computationally challenging to solve for arbitrary signals. To achieve a computationally efficient solution, we utilize a mixture-of-Gaussian (MoG) model to represent the FHSS signal. In our model, we uniformly divide the entire FHSS hopping range into L subbands. We denote the distribution of the signal within the l^{th} subband as $f_l(\mathbf{s}_{i,m}) = CN(\mathbf{0}, \mathbf{C}_{ss}^{(l)})$ and model it as a complex zero-mean Gaussian white signal with variance σ_s^2 within the l^{th} subband. Here, $\mathbf{C}_{ss}^{(l)}$ denotes the corresponding covariance matrix. The MoG model representing the FHSS signal in the *signal present* case is then given by

$$f(\mathbf{s}_{i,m}|\text{signal present}) = \sum_{l=1}^{L} P_l f_l(\mathbf{s}_{i,m}) \tag{3.30}$$

where P_l denotes the probability that the FHSS signal falls into the l^{th} subband at any given time.

Given the MoG model described in Equation 3.30 and row-wise normalized measurement matrix, the TSI optimization problem Equation 3.28 and gradient solution Equation 3.29 can be further reduced to:

$$\mathbf{\Phi}_{i,m} = \arg\max_{\hat{\mathbf{\Phi}}_{i,m}} H(\mathbf{y}_{i,m}|\text{signal present}),\ s.t\ \mathbf{y}_{i,m} = \hat{\mathbf{\Phi}}_{i,m}\mathbf{s}_{i,m} \tag{3.31}$$

and

$$\mathbf{\Phi}_{i,m}^{(j+1)} = \mathbf{\Phi}_{i,m}^{(j)} + \mu\nabla_{\mathbf{\Phi}_{i,m}} H(\mathbf{y}_{i,m}|\text{signal present}) \tag{3.32}$$

where $H(\mathbf{y}_{i,m}|\text{signal present})$ is the entropy of the measurement in the signal present case. Using Equation 3.30, the gradient of $H(\mathbf{y}_{i,m}|\text{signal present})$ is given by:

$$\nabla_{\mathbf{\Phi}_{i,m}} H(\mathbf{y}_{i,m}|\text{signal present}) \approx -\frac{\sum_{l=1}^{L} P_l |\mathbf{\Phi}_{i,m}\mathbf{C}_{xx}^{(l)}\mathbf{\Phi}_{i,m}^{\dagger}|^{-1} (\mathbf{\Phi}_{i,m}\mathbf{C}_{xx}^{(l)}\mathbf{\Phi}_{i,m}^{\dagger})^{-1} \mathbf{\Phi}_{i,m}\mathbf{C}_{xx}^{(l)\dagger}}{\sum_{l=1}^{L} P_l |\mathbf{\Phi}_{i,m}\mathbf{C}_{xx}^{(l)}\mathbf{\Phi}_{i,m}^{\dagger}|^{-1}} \tag{3.33}$$

with $\mathbf{C}_{xx}^{(l)} = \mathbf{C}_{ss}^{(l)} + \sigma_n^2 \mathbf{I}_{CR}$ and $\mathbf{I}_{CR}$ denoting the $CR \times CR$ identity matrix, and $|\cdot|$ denoting the determinant operator. Details of the derivations used to obtain this result are given in Appendix A.

3.3.1 Prior Knowledge Enhanced Measurement Kernel Design

In the above derivations, both the conditional entropy $H(\mathbf{y}_{i,m})$ and its gradient $\nabla_{\mathbf{\Phi}_{i,m}} H(\mathbf{y}_{i,m})$ are functions of the signal distribution, which can be represented by the subband usage probabilities P_l. Given knowledge of these subband usage probabilities P_l, TSI-optimal measurement kernels can be designed using the methods described above. If subband occupancy probabilities of the FHSS signal are known, a measurement kernel can be designed based on these probabilities. Since, in this case, our prior knowledge of the FHSS signal does not change during the entire observation process, the measurement kernel can be designed once and used throughout the observation process. More specifically, a one-time design of the measurement kernel $\mathbf{\Phi}_{i,m}$ can be performed and repeated it as the blocks in $\mathbf{\Phi}_i$ in the measurement matrix $\mathbf{\Phi}$ over the entire observation process.

3.3.2 Adaptive Measurement Kernel Design

Our final method discussed in this chapter is adaptive design of measurement kernels based on TSI optimization. In this approach, the measurement kernels $\mathbf{\Phi}_{i,m}$ are designed adaptively. After each measurement, a posterior probability of subband usage under the signal present assumption is calculated. This posterior probability is used to design the next measurement kernel. To calculate this

posterior probability, prior probabilities obtained from the previous observation periods and likelihood values computed using the measurements from the current observation period are used.

3.4 Results

Both theoretical analysis and simulations using practical signals were performed to evaluate the compressive detection performances of the systems discussed in this work. The results of these experiments are presented in this section.

We first compare the performances of the conventional detection system based on SSA and the compressive detection system with random measurement kernels. The theoretical FNR (i.e. probability of miss) calculated using the formulas derived earlier in this chapter versus signal-to-noise ratio (SNR) is shown in Figure 3.5. Here, the SNR is defined as:

$$SNR = \frac{\sigma_s^2}{\sigma_n^2} \tag{3.34}$$

In addition to the SSA and the proposed compressive detection with random measurement kernels, a clairvoyant system with knowledge of the FHSS hopping sequence was also implemented as reference. The clairvoyant system uses measurement kernels focused on the subband that the FHSS signal occupies at any time. Although unpractical, the clairvoyant system serves as a benchmark in the presented results. In Figure 3.5, the plots corresponding to four different α (relative scanning rate in SSA based detection systems and relative measurement rate in compressive detection systems) values are shown. The thresholds in the systems were obtained by setting the overall theoretical FPRs to 0.01. The results in this figure are for uniform channel usage of the FHSS signal, and corresponding to parameters $N_b = 20$ and $M = 16$.

In Figure 3.5, it is shown that the clairvoyant system, although unpractical, has the lowest probability of miss at all SNR and α values and serves as a benchmark. It is also shown that the conventional detection system based on SSA suffers from

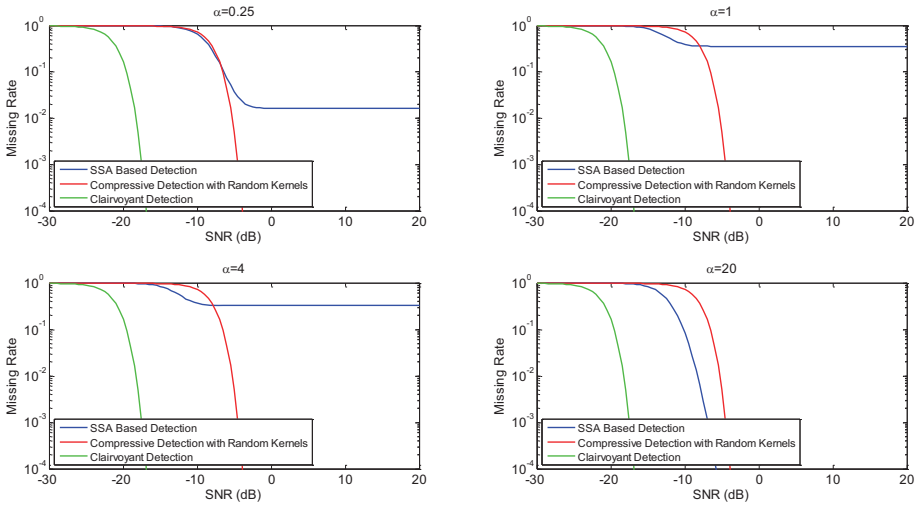

Figure 3.5: Comparison of Theoretical FHSS Detection Performances of Different Detection Systems

an evident "floor" in its FNR at high SNR values, if the relative scanning rate is not high enough. This floor results from the non-zero probability that the scanning support of SSA misses the hopping frequency of the FHSS signal in those cases. It can also be observed that the the compressive detection system with random measurement kernels has slightly higher FNR than the SSA based system at low SNR values due to the Noise Folding effect [48]. However, the compressive detection system does not suffer from the FNR "floor" problem as in the SSA based system and has a better performance than the SSA based system over a large range of SNR values.

A Monte-Carlo simulation study was also conducted to compare the performances of the detection systems. The FNR versus SNR obtained in these simulations are shown in Figure 3.6. The FHSS signals used in these simulations were similar to those specified in Subsection 2.2.1. In order to match the simulation setup to the theoretical analysis setup, we set $N_b = 20$. We specified 80 frequency channels and left the last channel unused. As a result, the number of frequency channels covered by a scanning subband was set to 4. Moreover, 4 symbol periods

were taken as a scanning interval in the SSA based detection system and an observation interval in the compressive detection system. Therefore, the number of Nyquist samples in each scanning/observation interval was 320. Different α values were obtained by varying the number of symbol periods per scanning/observation interval. A prewhitening step similar to the one discussed in Section 3.2 was applied to the measurements in the SSA based detection approach to counter the correlation introduced by the non-ideal filters used in the simulations. In the compressive detection system, the compression ratio (CR) was set to N_b so that the number of measurements during an observation interval in the compressive detection system is equal to the number of measurements during a scanning interval in the SSA based detection system. Similar to the theoretical results, the detection thresholds used in these systems were obtained by setting the overall theoretical FPRs to 0.01.

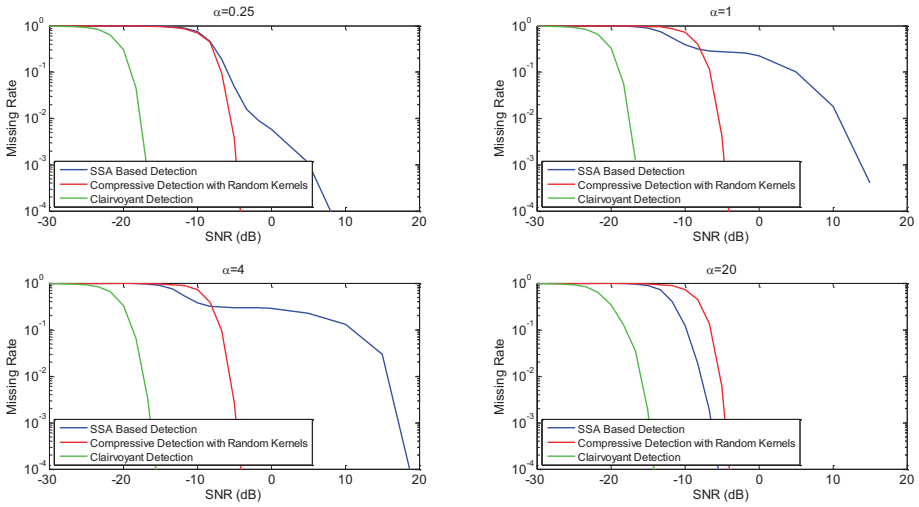

Figure 3.6: Comparison of Simulated FHSS Detection Performances of Different Detection Systems

In Figure 3.6, we can see that the simulated performances of the clairvoyant and the compressive detection systems match well with the results obtained by theoretical analysis in Figure 3.5. However, the FNR "floor" problem in the SSA

based system is somewhat diminished in Figure 3.6. This happens because of the usage of non-ideal filters in the practical simulations. With non-ideal filters, the signals outside the passband of the filters were not completely stopped. This unintentional leakage improved the detection performance of the SSA based detection system.

Next, we evaluate the performance of the compressive detection system with optimized measurement kernels using Monte Carlo simulations. Here, we consider the *static design* case where the measurement kernels are optimized once and used throughout the measurement process. The FHSS signals used in these simulations are almost the same as those used above except that we set $L = N_b = 20$ when designing measurement kernels and the prior distribution of the subband occupation is no longer uniform but follows the distribution shown in Figure 3.7. Similar to the experiments above, we set $CR = N_b$ for the compressive detection approaches and the thresholds in all systems are obtained by setting the overall theoretical FPRs to 0.01. The results are shown in Figure 3.8.

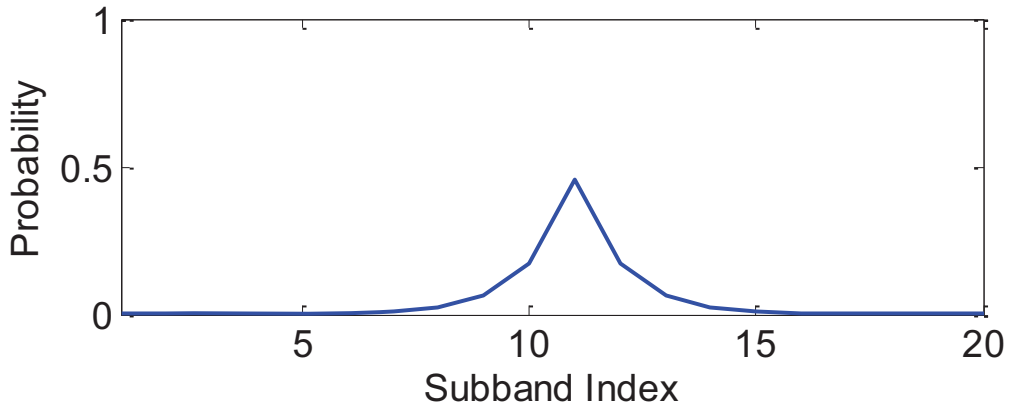

Figure 3.7: Prior Distribution of the Subband Occupation used in the Experiments

In Figure 3.8, the detection performance of the compressive detection system with prior knowledge enhanced measurement kernels is superior to that of the compressive detection system with random measurement kernels when the rela-

tive observation rate α is low. This improvement can be several orders of magnitude decrease in FNR. However, when the relative observation rate α is high, the performance of the compressive detection system with prior knowledge enhanced measurement kernels gets worse. Especially when $\alpha \geq N_b$ so that an FHSS hopping period covers the entire observation interval, the prior knowledge enhanced measurement kernels turn out to have worse performance than the random measurement kernels at high SNR values. This happens because as α increases, the spectra during the entire observation process becomes farther and farther away from that specified in Figure 3.7. As a result, the support of the prior knowledge enhanced measurement kernels are more likely to miss the signal in these cases.

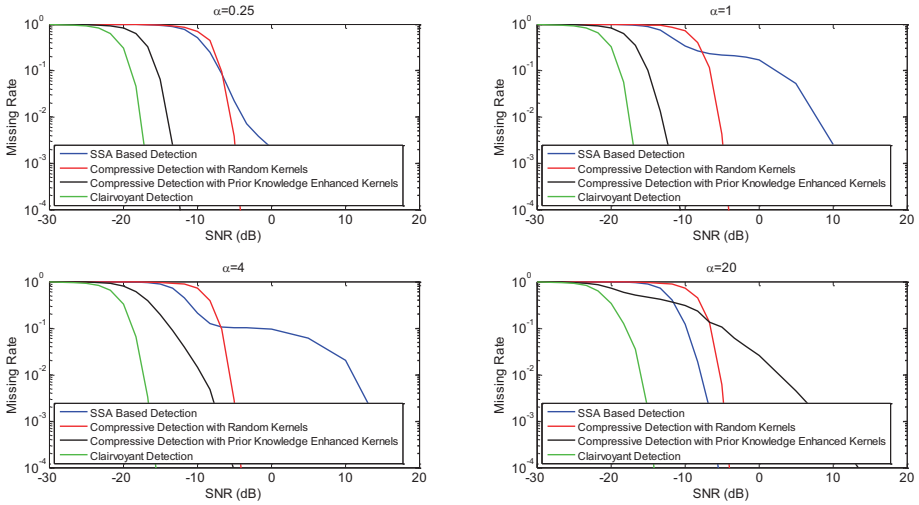

Figure 3.8: Comparison of Simulated FHSS Detection Performance of Compressive Detection System with Prior Knowledge Enhanced Measurement Kernels with other Detection Systems

The performance of the adaptive compressive detection approach was also evaluated using simulations. In these simulations, SNR was fixed to -5 dB which corresponds to an operating point where the prior knowledge enhanced compressive detection performs worse than the compressive detection approach with random measurement kernels according to Figure 3.8. We compare the FNRs of the adaptive compressive detection approach to the compressive detection approach with

random measurement kernels and the SSA based detection system after each observation/scanning interval. The detection decisions were made at the end of each observation interval using all the measurements from the first observation interval to the current observation interval. The thresholds were determined by setting the overall FPR to 0.01 with the measurements that had already been made. In the adaptive measurement kernel design, we initialized the first $1\times CR$ measurement kernel in the first observation interval $\mathbf{\Phi}_{1,1}$ to be from the prior knowledge enhanced measurement kernel assuming uniform subband occupation, and designed the remaining measurement kernels following Equations 3.32 and 3.33. We used almost the same setup of the FHSS signals as those used to obtain the results in Figure 3.6 except that we took the relative observation rate α to be large enough so that the frequency channel of the FHSS signal did not hop during the entire observation process. Therefore, the posterior distribution of the subband occupation of the FHSS signals remained valid since no frequency hopping took place.Similar to the simulations with prior knowledge enhanced measurement kernels, we set $L = CR = N_b = 20$. However, the distribution of the subband occupation in these simulations was taken to be uniform. The simulation results are shown in Figure 3.9. In the figure, Dwell Time denotes the number of observation intervals.

In Figure 3.9, we can observe that the FNR of the adaptive compressive detection system decreases faster than the compressive detection system with random measurement kernels. Therefore, much fewer observation intervals are needed for the adaptive compressive detection system to achive a particular FNR compared to the compressive detection system with random kernels. Similarly, after a given number of observation intervals, the adaptive compressive detection system has much lower FNR than the compressive detection system with random measurement kernels, and the improvement can be several orders in magnitude. Similar observations can also be made between the adaptive compressive detection and the SSA based detection system before the last observation interval. However, after the last observation interval, the performance of the SSA based detection system improves greatly since it has scanned all frequency channels. In fact, at $SNR = -5$

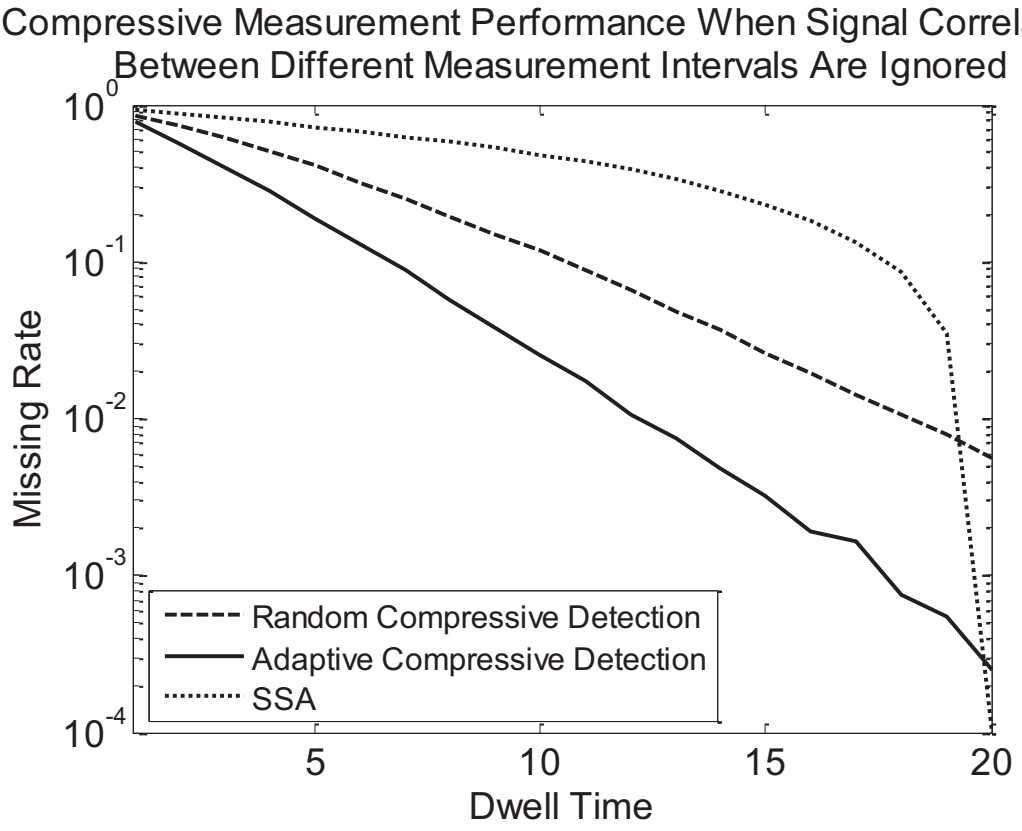

Figure 3.9: Comparison of Simulated FHSS Detection Performance of Adaptive Compressive Detection System with other Detection Systems

dB and after SSA has scanned all frequency channels, the performance of the SSA based detection system is slightly better than the adaptive compressive detection system. However, we don't expect this behaviour to hold at higher SNR values. According to the theoretical performance equations presented earlier in this chapter, the *random* compressive detection has better performance than the SSA based detection system when the SNR is higher than -2.45 dB. Since the detection error rates at these SNR values are very small, hundreds of millions of Monte-Carlo simulations are needed to evaluate the performance of detection systems by simulations. The computational complexity of these simulations are beyond our computational resources at this time. However, since adaptive compressive detection outperforms compressive detection with random kernels, we expect the adaptive compressive

detection to outperform the SSA based detection system at SNRS higher than -2.45 dB, even after the SSA has the chance to scan all frequency channels.

3.5 Summary and Conclusions

In this chapter, we proposed methods for non-cooperative compressive detection of FHSS signals. We provided an introduction to the FHSS detection problem and reviewed existing methods. We then introduced a compressive detection approach that used random measurement kernels. In addition to the compressive detection system with random measurement kernels, we also introduced a compressive detection system with designed measurement kernels. We proposed the use of an information theoretic metric called TSI to design the measurement kernels. Finally, we illustrated how the measurement kernels could be adapted during the measurement process. The proposed detection methods were evaluated using both theoretical analysis and simulations using practical FHSS signals. The theoretical and experimental results revealed that the proposed compressive detection methods could provide advantages over conventional methods. The compressive detection systems did not suffer from the FNR "floor" problem which was observed in SSA based systems when the relative scanning rate was low and the SNR was high. In addition, experimental results also illustrated that prior (or posterior) knowledge of signal distribution could be used to design measurement kernels which yielded enhanced detection performance compared to random measurement kernels.

CHAPTER 4

COMPRESSIVE DETECTION OF DIRECT SEQUENCE SPREAD SPECTRUM SIGNALS

In this chapter, we introduce non-cooperative compressive detection methods to detect the presence of DSSS signals. We start by providing an overview of existing presence detection methods for DSSS signals. The two most common class of detection methods are based on energy detection and autocorrelation. We propose compressive approaches for both of these detection strategies. Similar to Chapter 3, we consider both random measurement kernels as well as knowledge enhanced measurement kernels. Theoretical and experimental results are provided to compare the proposed approaches with conventional methods and conclusions are drawn at the end of the chapter.

4.1 Introduction

As discussed in Section 2.2.2, DSSS signals spread the spectrum of the original input signal by modulating the signal with a pseudorandom chip sequence. The resulting signal spectra is spread over a wider bandwidth and detecting the presence of a DSSS signal without the knowledge of the spreading sequence becomes a challenging task. Although many types of methods have been proposed (e.g. higher-order statistics [49], PCA based analysis [50], neural networks [51]) to address DSSS detection in the literature, the two most common types of approaches are based on energy detection or autocorrelation detection.

Energy detection methods [52, 53] rely on calculating the signal energy over a period of time and comparing this energy to a threshold. Due to modulation by a PN sequence, the DSSS signal appears as noise to non-cooperative receivers. Therefore, an increase in measured energy level at the detector input is attributed

to the presence of a DSSS signal.

Autocorrelation-based DSSS detection [54–58] methods utilize the autocorrelation function of DSSS signals. Since PN sequences are binary sequences with certain chip rates and DSSS signals (especially SC-DSSS signals) are modulated repetitions of PN sequences, autocorrelation of DSSS signals exhibit cyclostationarity. Autocorrelation based methods are specifically developed to exploit these cyclostationary features of DSSS signals.

In the following sections, we provide details of these two conventional approaches for DSSS detection. Each section discussing a conventional method is followed by another section introducing a new compressive method using the same approach.

4.2 Conventional Energy-Based Detection of Direct Sequence Spread Spectrum Signals

In this section, we discuss the conventional energy-based detection methods for DSSS signals using the framework illustrated in Figure 4.1. In this framework, the DSSS signal $\mathbf{s}$ is corrupted by additive channel noise $\mathbf{n}$. A prefilter is applied to the noisy signal at the input of the receiver to remove the frequency components outside of the spectrum of interest. The prefiltered signal is integrated and sampled at the Nyquist rate of the DSSS signal. Note that the effects of quantization noise, denoted by n_s, are ignored in our analysis. Denoting the bandwidth of the DSSS signal by B, the Nyquist sampling rate is given by $2B$. The detection decision is made by thresholding the energy of the measurement vector $\mathbf{y}$.

To build a discrete model of this system, consider the signal $\mathbf{s}$ to denote the vector obtained by sampling the signal $\mathbf{s}$ at its Nyquist rate $2B$ and $\mathbf{n}$ to denote the discrete additive noise vector. The detection decision can then be made by

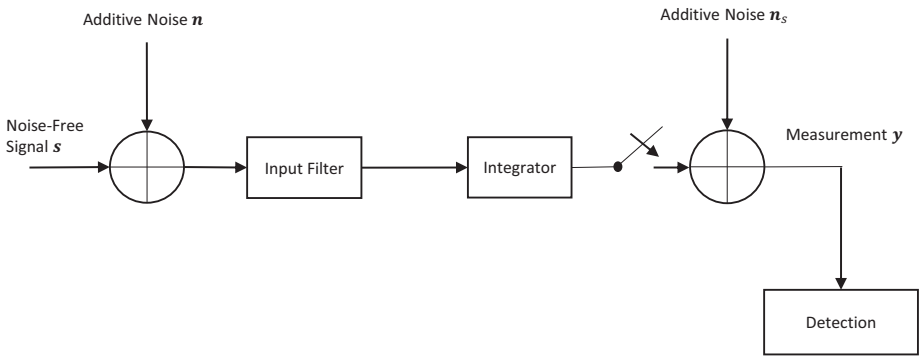

Figure 4.1: Conventional Energy Based Detector of DSSS Signals

deciding between two hypotheses:

$$H_0 : \mathbf{y} = \mathbf{n} \tag{4.1}$$

$$H_1 : \mathbf{y} = \mathbf{s} + \mathbf{n} \tag{4.2}$$

where H_0 and H_1 denote the hypotheses corresponding to the signal absent and signal present cases, respectively.

We model $\mathbf{s}$ as a zero-mean Gaussian white signal with variance σ_s^2 and $\mathbf{n}$ as zero-mean Gaussian white noise with variance σ_n^2 over the DSSS signal spectrum. Let N_{samp} denote the number of samples (i.e. the dimension of the measurement vector $\mathbf{y}$). The distribution of the energy of $\mathbf{y}$, denoted by λ, in the signal absent case is then given by:

$$pr(\lambda|\text{signal absent}) = \frac{\lambda^{(N_{samp}-1)} e^{-\frac{\lambda}{{\sigma_n}^2}}}{{\sigma_n}^{2N_{samp}} \Gamma(N_{samp})} \tag{4.3}$$

Similarly, the distribution of λ in the signal present case is given by:

$$pr(\lambda|\text{signal present}) = \frac{\lambda^{(N_{samp}-1)} e^{-\frac{\lambda}{({\sigma_s}^2+{\sigma_n}^2)}}}{({\sigma_s}^2 + {\sigma_n}^2)^{N_{samp}} \Gamma(N_{samp})} \tag{4.4}$$

The detection is performed by thresholding the signal energy λ. Given a threshold T, the theoretical false positive rate and the theoretical false negative rate of the system are calculated using Equations 3.23 and 3.24, respectively.

4.3 Energy-Based Compressive Detection of Direct Sequence Spread Spectrum Signals

In this section, we propose energy-based compressive detection methods for DSSS signal detection. Detection methods using both random and knowledge enhanced measurement kernels are discussed. The methods presented in this section share the same compressive detection framework introduced in Section 3.2 and the block diagram of this detection framework was shown in Figure 3.2.

Similar to our analysis in Section 3.2, we divide the entire observation period into N_b sequential observation intervals. Since wide-band measurement kernels are used in this system, the final detection decision is made using all measurements collected during the entire observation process to decide between two hypotheses:

$$H_0 : \mathbf{y} = \mathbf{\Phi n} \tag{4.5}$$

$$H_1 : \mathbf{y} = \mathbf{\Phi}(\mathbf{s} + \mathbf{n}) \tag{4.6}$$

where H_0 and H_1 denote the signal absent and signal present hypotheses, respectively. $\mathbf{\Phi}$ denotes the $MN_b \times NN_b$ measurement matrix representing the measurement kernels used during the entire observation period. Referring to Section 4.2, $N_{samp} = NN_b$ denotes the number of samples used to represent the input signal at the Nyquist rate. Note that $\mathbf{\Phi}$ is block diagonal with each $M \times N$ diagonal block $\mathbf{\Phi}_i$ representing the measurement kernel during the observation interval i ($1 \leq i \leq N_b$). The structure of each $\mathbf{\Phi}_i$ is also block diagonal as shown in Figure 3.3. The measurement, the signal, and the channel noise during the i^{th} observation interval are denoted by $\mathbf{y}_i$, $\mathbf{s}_i$ and $\mathbf{n}_i$, respectively. These vectors are concatenated over N_b observation intervals to form $\mathbf{y}$, $\mathbf{s}$, and $\mathbf{n}$, respectively. A prewhitening step (as

described previously by Equations 3.19 and 3.20) is applied to the measurements obtained during the ith observation interval $\mathbf{y}_i$ to yield $\widetilde{\mathbf{y}}_i$. The vectors $\widetilde{\mathbf{y}}_i$ are used to form the prewhitened measurement vector $\widetilde{\mathbf{y}}$ which contains the prewhitened measurements for the entire observation period.

The final detection decision is made by thresholding the energy of prewhitened compressive measurement vector $\widetilde{\mathbf{y}}$. For the compressive energy-based detection with random measurement kernels, we model the signal $\mathbf{s}$ as zero-mean Gaussian white with variance σ_s^2 and the channel noise $\mathbf{n}$ as zero-mean Gaussian white with variance σ_n^2 over the entire DSSS spectrum. The theoretical performance of this detector can be analyzed using the distributions of the energy for the signal absent and signal present cases which are given by the Equations 3.21 and 3.22, respectively. The corresponding FPR and FNR are then calculated using Equations 3.23 and 3.24, respectively.

4.3.1 Energy-Based Knowledge Enhanced Compressive Detection of Direct Sequence Spread Spectrum Signals

Next, we discuss knowledge enhanced measurement kernel design methods for energy-based compressive detection of DSSS signals. The methods discussed in this section follow the principles discussed in Section 3.3. Our goal is to design measurement kernels that will maximize TSI which we define as the mutual information between the DSSS signal and the measurements. In our analysis, we make a simplifying assumption and assume that the receiver has symbol period synchronization. Under this assumption, each observation interval is set equal to a symbol period and the measurement kernels are designed for each symbol period. Similar to the FHSS design in Section 3.3, the measurement matrix has a block-diagonal structure and the m^{th} block of the measurement matrix during the i^{th} measurement interval is denoted by $\mathbf{\Phi}_{i,m}$.

To obtain a sparse representation of the DSSS signal, we form an $N_s \times K$ dictionary $\mathbf{\Psi}_s$. N_s denotes the number of Nyquist samples in each symbol period

and K denotes the number of possible PN sequences. The columns of the matrix $\mathbf{\Psi}_s$ are formed by the PN sequences sampled at the highest possible Nyquist rate. Note that the DSSS signal during each symbol period can be represented using this dictionary with sparsity of 1.

The measurement kernel design is performed by maximizing the TSI between the DSSS signal and the measurements using Equation 3.25. As discussed in Section 3.3, this optimization can be computationally challenging for arbitrary signals. Therefore, we again utilize a MoG model to represent the DSSS signal in order to simplify the optimization task. For the signal present case, the distribution of the signal $\mathbf{s}_{i,m}$ during the i^{th} measurement interval and m^{th} observation interval is given by the Gaussian mixture

$$f(\mathbf{s}_{i,m}|\text{signal present}) = \sum_{l=1}^{K} P_l f_l(\mathbf{s}_{i,m}) \tag{4.7}$$

where $f_l(\mathbf{s}_{i,m}) = CN(\mathbf{0}, \mathbf{C}_{ss}^{(i,m,l)})$ is a complex zero-mean Gaussian white distribution with the covariance matrix $\mathbf{C}_{ss}^{(i,m,l)}$. Note that each mixture element in Equation 4.7 represents one atom of the dictionary $\mathbf{\Psi}_s$ and, thus, corresponds to one possible PN sequence. Therefore, the covariance matrix $\mathbf{C}_{ss}^{(i,m,l)} = \psi_s^{(i,m,l)}(\psi_s^{(i,m,l)})^H$, where $\psi_s^{(i,m,l)}$ denotes the l^{th} atom of the dictionary $\mathbf{\Psi}_s$ during the i^{th} measurement interval and m^{th} observation interval. In Equation 4.7, P_l denotes the probability that a signal corresponding to the l^{th} PN sequence is transmitted. Given prior probabilities of PN sequence usage, prior knowledge enhanced measurement kernel design can be performed by following Equation 3.32 and Equation 3.33.

It is also possible to extend this framework to allow adaptive measurement kernel design. After each measurement, a posterior probability of PN sequence usage under the signal present assumption is calculated. This posterior probability is used to design the next measurement kernel. The posterior probabilities are calculated using prior probabilities from previous observation periods and likelihood values computed using the measurements from the current observation period.

4.4 Conventional Autocorrelation-Based Detection of Direct Sequence Spread Spectrum Signals

In this section, we discuss methods that detect the presence of DSSS signals by exploiting the properties of their autocorrelation function. Many such methods have been reported in the literature [58–60]. Compared to the energy-based detection methods, these methods may require additional prior knowledge such as the symbol period, chip period, or the DSSS signal spectrum. In addition, the systems that implement these methods are generally more complex than their energy-based counterparts due to the need for computing the autocorrelation function.

In our discussion, we will consider the method introduced in [59,60], which only assumes the knowledge of symbol period T_s. The system block diagram for this method is shown in Figure 4.2.

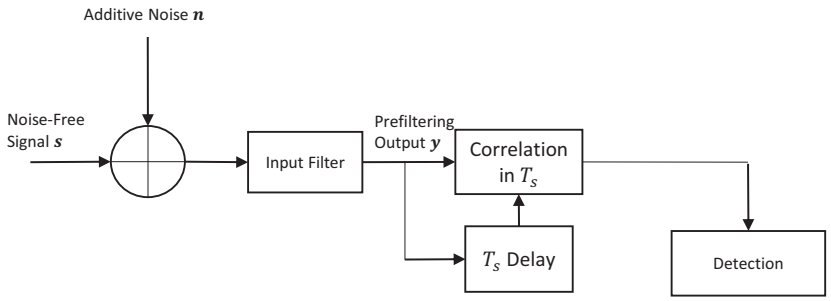

Figure 4.2: Conventional Autocorrelation-Based Detector for DSSS Signals

In this framework, a prefiltering step is used first to remove the frequency components that are outside of the DSSS spread spectrum range. The prefiltered

signal is then delayed by the symbol period T_s and correlated with itself. Given a correlation interval T_c, the output of the correlator can be expressed as

$$\hat{R}_i = \frac{1}{T}\int_{t_i}^{t_i+T_c} y(t)y^*(t-T_s)dt \tag{4.8}$$

where $y(t)$ and $y^*(t)$ denote the prefiltered signal and its complex conjugate, respectively and t_i notes the start time of the correlation period. Since we focus on discrete systems in this work, we will consider that the prefiltered signal is sampled at the Nyquist sampling rate to yield its discretized version $\mathbf{y}$. The number of samples taken at the Nyquist rate during the intervals T_c and T_s are denoted by N_c and N_s, respectively.

The detection decision is made by deciding between two hypotheses:

$$H_0 : \mathbf{y} = \mathbf{n} \tag{4.9}$$

$$H_1 : \mathbf{y} = \mathbf{s} + \mathbf{n} \tag{4.10}$$

where H_0 and H_1 denote the hypotheses corresponding to the signal absent and signal present cases, respectively. This decision is made by thresholding the mean value of the squared correlation value over N_b observation intervals

$$\lambda = \frac{1}{N_b}\sum_{i=1}^{N_b} \hat{R}_i^2. \tag{4.11}$$

We model the channel noise as additive zero-mean Gaussian white noise with variance of σ_n^2 over the entire spread spectrum range. In the signal absent case, the distribution of λ is given by

$$pr(\lambda|\text{signal absent}) = \frac{(\frac{\lambda}{N_b})^{(N_b-1)} e^{-\frac{\lambda}{N_b {\sigma_{nc}}^2}}}{N_b {\sigma_{nc}}^{2N_b}\Gamma(N_b)} \tag{4.12}$$

where $\sigma_{nc}^2 = \frac{\sigma_n^4}{N_c}$. In the signal present case, the distribution of λ is given by

$$pr(\lambda|\text{signal present}) = \frac{(\frac{\lambda}{N_b})^{(N_b-1)} e^{-\frac{\lambda}{N_b(\sigma_{sc}^2+\sigma_{nc}^2)}}}{N_b(\sigma_{sc}^2+\sigma_{nc}^2)^{N_b}\Gamma(N_b)} \tag{4.13}$$

where σ_s^2 denotes the signal power and $\sigma_{sc}^2 = \frac{N_s \sigma_s^4}{N_c}$. Equation 4.13 assumes that the observation interval T_c is sufficiently long compared to the symbol period T_s. Given these distributions and a threshold T, the theoretical false positive and false negative rates can be calculated using Equations 3.23 and 3.24.

4.5 Autocorrelation-Based Compressive Detection of Direct Sequence Spread Spectrum Signals

In this section, we introduce compressive methods for autocorrelation-based detection of DSSS signals. The proposed compressive detection framework is illustrated in Figure 4.3. In contrast to the conventional system shown in Figure 4.2, this system makes compressive measurements on the prefiltered input signal. The sampling rate used for the compressive measurements is significantly lower than the Nyquist rate used for the system in Figure 4.2.

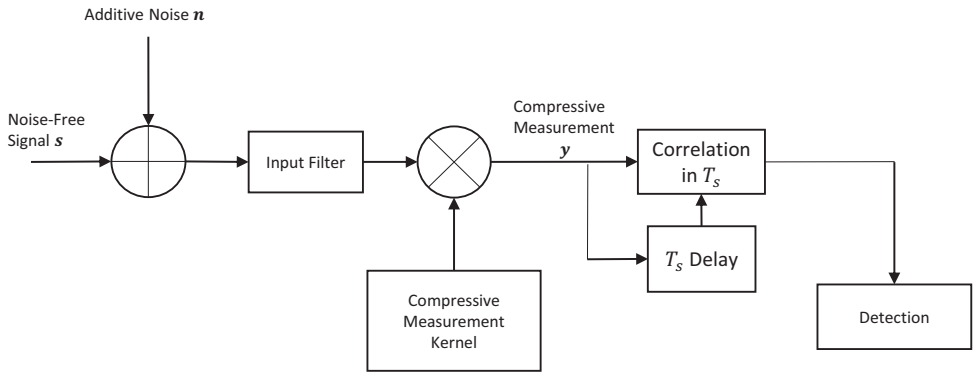

Figure 4.3: Compressive Autocorrelation-Based Detector for DSSS Signals

The detection decision in this system is made by deciding between two hypotheses

$$H_0 : \mathbf{y} = \mathbf{\Phi n} \tag{4.14}$$

$$H_1 : \mathbf{y} = \mathbf{\Phi}(\mathbf{s} + \mathbf{n}) \tag{4.15}$$

The notation and major steps of this analysis are similar to those presented in Section 4.3 with a few notable exceptions: In order to maintain the cyclostationary properties of the signals in our compressive measurements, we fix the measurement kernels during each measurement interval. In addition, we aim to minimize dependencies between autocorrelation measurements. Therefore, we set the measurement intervals to be apart by a symbol period T_s so that the calculation of autocorrelation during each measurement period does not involve compressive measurements from other measurement intervals. To express this condition numerically, let T_m denote the measurement interval. We set

$$T_m = T_c + T_s \tag{4.16}$$

where T_c denotes the observation interval for autocorrelation computations as was shown in Equation 4.8. Under this condition, the number of Nyquist samples during a measurement period N is given by

$$N = N_c + N_s \tag{4.17}$$

with N_c and N_s denote the number of Nyquist samples in T_c and T_s, respectively. Similarly, the number of compressive measurements during the measurement interval T_m is given by

$$M = M_c + M_s \tag{4.18}$$

where M_c and M_s denote the number of compressive measurements in T_c and T_s, respetively. The ratio $\frac{N}{M}$ is the compression ratio CR.

The final detection decision is made by thresholding the mean of the squared correlation over N_b of disjoint observation intervals. For the signal absent case, the

distribution of this mean-squared correlation λ is given by

$$pr(\lambda|\text{signal absent}) = \frac{(\frac{\lambda}{N_b})^{(N_b-1)} e^{-\frac{\lambda}{N_b {\sigma_{mnc}}^2}}}{N_b {\sigma_{mnc}}^{2N_b} \Gamma(N_b)} \tag{4.19}$$

where $\sigma^2_{mnc} = \frac{\sigma_n^4}{R_c}$. For the signal present case, the distribution is given by

$$pr(\lambda|\text{signal present}) = \frac{(\frac{\lambda}{N_b})^{(N_b-1)} e^{-\frac{\lambda}{N_b(\sigma^2_{msc}+\sigma^2_{mnc})}}}{N_b(\sigma^2_{msc}+\sigma^2_{mnc})^{N_b} \Gamma(N_b)} \tag{4.20}$$

where $\sigma^2_{sc} = \frac{R_s \sigma_s^4}{R_c}$. R_s and R_c denote the ranks of the matrix representation of the measurement kernels in time intervals T_s and T_c, respectively. It should be noted that the Equation 4.20 was derived under the assumption that T_c is significantly longer than T_s. Given these distributions and a threshold T, the theoretical false positive and false negative rates can be calculated using Equations 3.23 and 3.24, respectively.

4.5.1 Autocorrelation-Based Knowledge Enhanced Compressive Detection of Direct Sequence Spread Spectrum Signals

The methods used to perform knowledge enhanced compressive detection using autocorrelation are largely similar to the methods introduced earlier for energy-based methods in Section 4.3.1 with one notable exception: As discussed in the previous section, within one measurement interval, the measurement kernel is kept constant. Therefore, the adaptation occurs only across measurement intervals and not within a measurement interval. With this exception, the design procedure is the same as described in Section 4.3.1 .

4.6 Results

In this section, we present theoretical and experimental results for non-cooperative detection of DSSS signals. Similar to the FHSS detection experiments in Chapter 3, both theoretical analysis and simulations with practical signals were performed.

First, we compare the performances of the conventional detection systems based on energy detection and autocorrelation with their compressive counterparts using random measurement kernels. The DSSS signals used here are the SC-DSSS signals described in Subsection 2.2.2. The parameters used in these experiments were determined as follows: The Nyquist sampling rate was defined with respect to the largest spread bandwidth among all possible signals. In this case, the number of Nyquist samples in a symbol period of the signals was $N_s = 62$. To compare the systems, we considered 20 symbol periods. For the non-compressive energy-based detection system, this resulted in $N_{samp} = 62{\times}20 = 1240$. For the remaining system, we set $N_b = 4$ which meant that each observation interval contained 5 symbol periods. This selection resulted in $62{\times}5 = 310$ Nyquist samples. During each symbol period, we first used 12 compressive measurements which resulted in a compression ratio of $\frac{62}{12} = 5.167$. While keeping the compression ratio constant at 5.167, we repeated these experiments for 80 and 200 symbol periods with $N_b = 4$ and $N_b = 10$, respectively.

Assuming equal usage probabilities for all possible PN sequences, the theoretical False Negative Rate (FNR) (i.e. probability of miss) was calculated using the formulas given earlier in this section. The FNR values vs SNR are plotted in Figure 4.4. The thresholds in all systems were obtained by setting the overall theoretical False Positive Rates (FPRs) to 0.01.

In Figure 4.4, we observe that the detection performance of all systems improve with increasing SNR. Importantly, we also observe that the compressive detection systems deliver a reasonable trade-off between detection performance and hardware cost. For example, using roughly one fifth of the measurements, the energy-based compressive detection system requires roughly 3 dB increase in SNR to achive the same FNR value as the uncompressed system. We can also observe that auto-correlation based detection systems provide worse detection performance than the energy-based ones. This is because the number of samples at the output of the correlator is much smaller than the number of samples used in energy calculations.

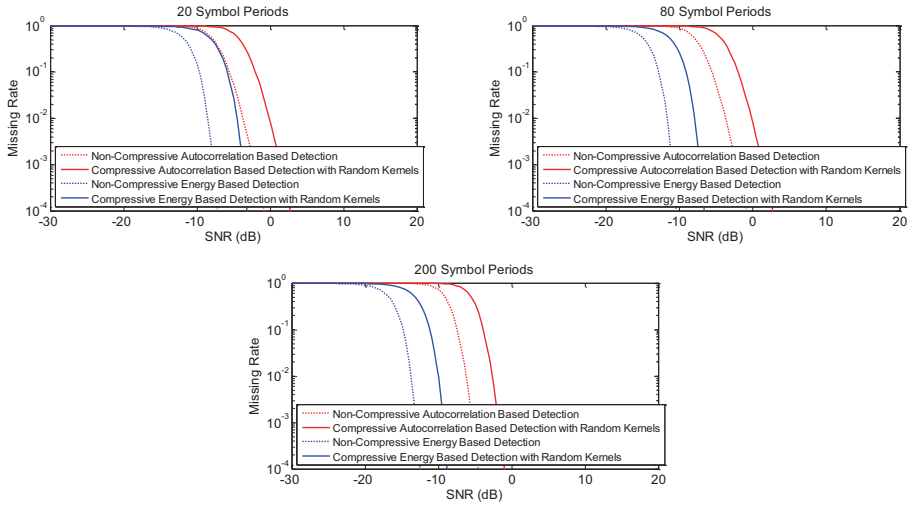

Figure 4.4: Comparison of Theoretical DSSS Detection Performance

We speculate that the fewer number of samples used in the calculations reduces the statistical accuracy of the autocorrelation methods.

In order to compare the theoretical performance of the systems to simulated performance, we performed simulations using the same experimental setup as was used for the results shown in Figure 4.4. The results obtained from these simulations are shown in Figure 4.5. Comparing Figure 4.5 to Figure 4.4, we observe that the simulated performances of the conventional non-compressive detection systems and their compressive implementations with random kernels match very well with the theoretical analysis.

Next, we evaluate the performances of prior knowledge enhanced compressive detection systems using simulations. The experimental set-up in these simulations was almost identical to that used to generate Figures 4.4 and 4.5, except that the prior distribution of the PN sequence usage was modified as shown in Figure 4.6, where PN sequences with higher orders have higher indices on the x-axis. The results of these simulations are shown in Figure 4.7. In the figure, we can observe that using the prior knowledge enhanced measurement kernels, the detection performanced of the compressive detection systems improves significantly in com-

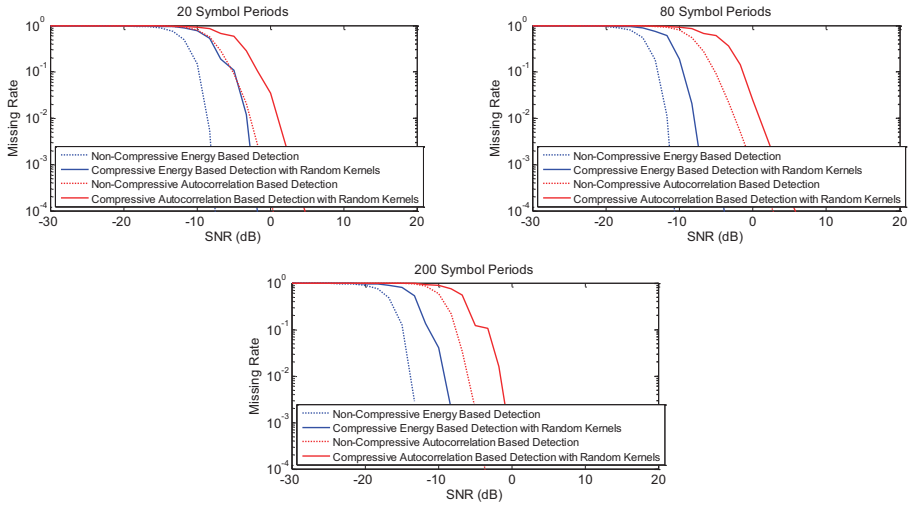

Figure 4.5: Comparison of Simulated DSSS Detection Performance

parison to the systems with random measurement kernels. In fact, we can also observe that the detection performances of these systems are almost as good as those achieved by non-compressive detection systems. This is especially true for the autocorrelation-based systems.

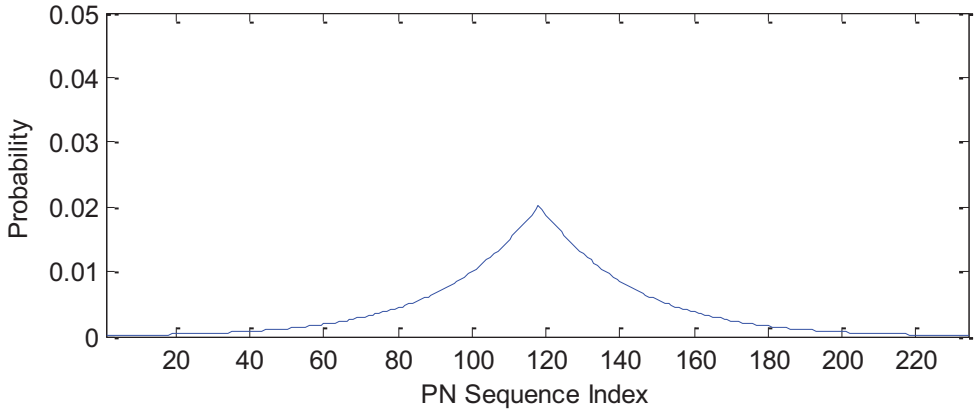

Figure 4.6: Prior Distribution of the PN Sequence Usage

Simulations were also performed to evaluate the performances of adaptive compressive detection methods. In these simulations, SNR was -5 dB. 20 symbol periods were used in these experiments and the compression ratio was $\frac{62}{12} = 5.167$

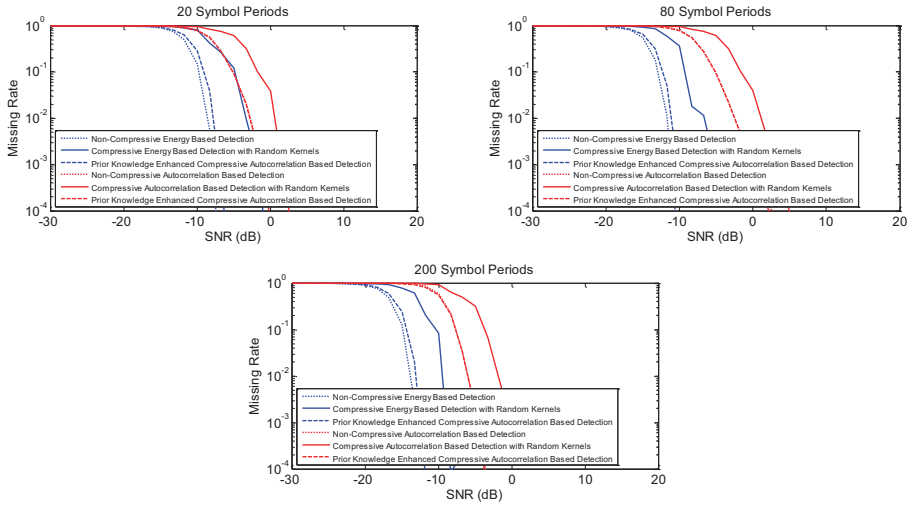

Figure 4.7: Comparison of Simulated DSSS Detection Performances of Compressive Detection Systems with Prior Knowledge Enhanced Measurement Kernels with other Detection Systems

as in previous experiments. A decision was made after each 5 symbol period using thresholds corresponding to theoretical $FPR = 0.01$ at each decision time. For the adaptive detection systems, the non-zero entries of the first row in the measurement matrix was initialized using the values of the prior knowledge enhanced measurement kernel assuming equal PN sequence usage probabilities. The detection performance comparison of the non-compressive detection systems, their compressive implementations with random measurement kernels and adaptive compressive detection implementations are shown in Figure 4.8, In this figure, the dwell time denotes each decision time.

In Figure 4.8, we can observe that the detection performance of the adaptive autocorrelation-based compressive detection system improves significantly in comparison to the detection performance of the compressive system with random measurements. However, what is even more notable is the performance of the adaptive energy-based compressive detection system. The FNR of this system is so low that no errors were observed in more than $20,000$ simulations used to generate the

results on this plot. Thus, the curve for this system is not displayed on this plot. This is particularly notable since the performance of this adaptive system is even superior to that obtained using the corresponding non-compressive system.

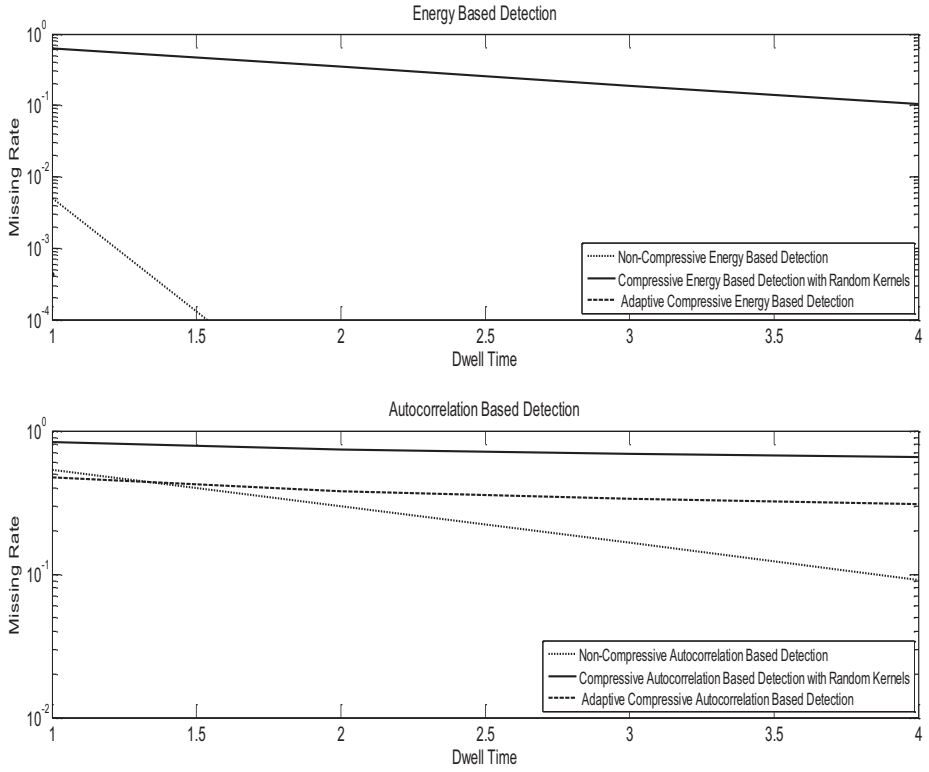

Figure 4.8: Comparison of Simulated DSSS Detection Performances of Adaptive Compressive Detection Systems with other Detection Systems

4.7 Summary and Conclusions

In this chapter, we proposed methods for non-cooperative compressive detection of DSSS signals. We started by introducing two conventional DSSS detection approaches; one based on energy and another one based on autocorrelation. We then introduced compressive implementations of both methods using random measurement kernels. In addition to the compressive detection systems with random mea-

surement kernels, we also discussed compressive detection systems with designed measurement kernels. Finally, we illustrated how the measurement kernels could be adapted during the measurement process. Theoretical and experimental results illustrated that the compressive implementations were competitive with their non-compressive counterparts. In fact, our results suggested that energy-based adaptive compressive detection system could outperform its non-compressive counterpart.

CHAPTER 5

COMPRESSIVE DECODING OF SPREAD SPECTRUM SIGNALS

In this chapter, we introduce our proposed non-cooperative compressive decoding methods for SS signals, which can be implemented for both FHSS and DSSS signals. We firstly review the background literatures. Then the motivations and system setup are introduced. Later, we discuss about the implementation of the random measurement kernels and the knowledge enhanced methods in compressive decoding of SS signals, including the prior knowledge enhanced compressive decoding and the adaptive compressive decoding with posterior knowledge from the measurements that have already been made. Moreover, some further improvement of the decoding systems are proposed. Then, we discuss about the implementations for both the FHSS and the DSSS signals as examples of SS signals. After that, experimental results are shown and discussions are given. Finanlly, summary and conclusions for this chapter are drawn.

5.1 Background of Decoding of Spread Spectrum Signals

In this section, we review the existing literatures on the decoding of the SS signals. The decoding algorithms of FHSS signals and DSSS signals can be treated as the decoding of band limited communication algorithms. Conventionally, Nyquist rate with respect to the entire SS spectrum is used in the decoding problem. However, this is expensive and sometimes even impossible. So compressive methods are proposed in a lot of literatures.

In most of the existing works, compressive decoding of communication signals related to spread spectrum were done without adaptation. [61–66] had discussions on the sensing system structure or sensing matrix improvement before the sens-

ing process started. In [67], learned dictionaries based on K-SVD algorithm was adopted to improve the performance of the compressive sensing reconstructions. But none of the above included sensing adaptations based on previous measurements. [68] was relative to sensing adaptation, but factually, it was just about a judgment of finding a good reconstruction without the adaptive design of the measurement kernels. However, we find that most of those communication compressive sensing systems were established using a weighted (the weight sequence is called sampling sequence) continuous-to-discrete converter working as a sampler with its sampling rate much lower than the Nyquist rate.

In the decoding part from compressive measurements, most literatures suggested reconstructing the signal first and do the detection task based on the reconstructed signals [61, 64–69]. People also proposed detection algorithms without reconstruction of the signals based on matched filtering by establishing dictionaries to make the sparisty of the signals to be 1 or 2 [70–74], which had a similar idea to the compressive matched filter introduced in [75]. In this work, our compressive decoding approaches are developed without reconstruction of the original signals.

5.2 System Set-up and Compressive Decoding with Random Measurement Kernels

5.2.1 System Set-up

The receiver of our proposed compressive decoding approaches of SS signals is similar to that used for compressive energy based presence detection. Its framework is modeled in Figure 5.1, where the input is received noise-free continuous signal, and the output is the measurement of the sensing system.

In Figure 5.1, the integrator can be implemented using a low-pass filter and the switch in the system operates at the required compressive sampling rate. With those two components, the continuous input signals are converted to temporally

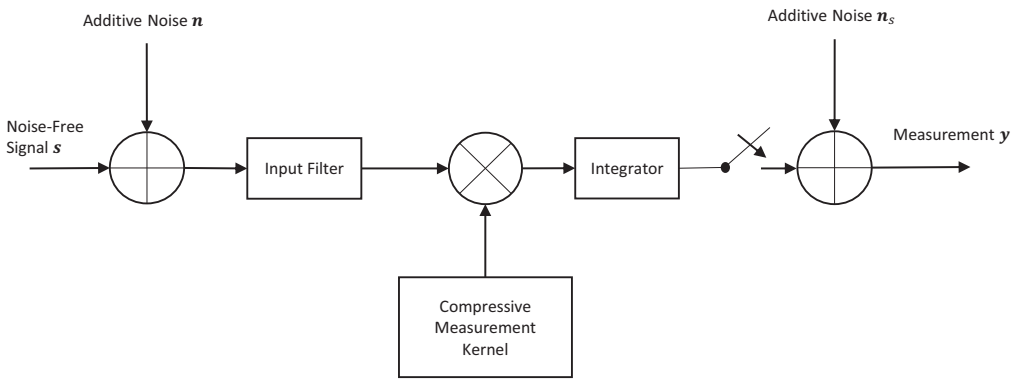

Figure 5.1: Achitecture of Compressive Sensing of Spread Spectrum Signals

discrete signals. For the conventional approach, the operating rate of the switch is the Nyquist rate with the regard of the entire spread spectrum range. However, to make it more feasible and less expensive, we lower down the rate and vary the sampling code to make it a compressive decoding system.

With the above setup, the sensing part of the compressive decoding in a symbol period in this application can be modeled as:

$$\mathbf{y} = \mathbf{\Phi}(\mathbf{s} + \mathbf{n}) \tag{5.1}$$

where $\mathbf{\Phi}$ is the $M \times N$ dimensional sensing matrix; $\mathbf{s}$ is the input discretized received noise-free signal; and $\mathbf{n}$ is the additive Gaussian noise vector to the input signal. Because the effect of the additive noise to the measurement $\mathbf{n}_s$ is much smaller than to the input signal $\mathbf{n}$, we ignore $\mathbf{n}_s$ in our analysis, and the same assumption is used for the rest of the chapter. Similar to Chapter 3 and Chapter 4, we still define the compression ratio (CR) to be the ratio of the Nyquist sampling rate with respect to the entire spread spectrum range to the compressed sampling rate, and

define the signal-to-noise ratio (SNR) to be the ratio of the power of $\mathbf{s}$ to the power of $\mathbf{n}$.

For the sensing system described in Figure 5.1, $\mathbf{\Phi}$ is a block diagonal matrix with each block as a row vector, similar to that discussed in Chapter 3.

Compressive sensing states that if a signal can be sparsely represented based on some "dictionary", it can be linearly sensed with a lower rate than Nyquist rate and reconstructed with overwhelmed probability. With the consideration that for SS signals, there are only a finite number of possible signals within each symbol period, we can sparsely represent the SS signals with 1 sparse degree based on the dictionary composed by all the possible signals in one symbol period.

To model the system in a discrete to discrete (DD) system, we mathematically discretize the input signal in each symbol period with a rate not lower than the Nyquist rate. Assuming the dimension of the input discretized signal is $N\times1$ and there are $2K$ possible signals (The first K signals with the symbol content of 0 and the second K signals with the symbol content of 1), we can sparsely represent the input discretized noise-free signals in one symbol period as:

$$\mathbf{s} = \mathbf{\Psi}\vartheta \tag{5.2}$$

where $\mathbf{\Psi}$ is the $N\times2K$ sized dictionary; and ϑ is a $2K\times1$ sized binary vector with only 1 entry to be nonzero (i.e. sparsity is 1), which select a signal from the dictionary matrix.

From 5.1 and 5.2, we have:

$$\mathbf{y} = \mathbf{\Phi}(\mathbf{\Psi}\vartheta + \mathbf{n}) = \mathbf{\Phi}\mathbf{\Psi}\vartheta + (\mathbf{\Phi}\mathbf{n}) \tag{5.3}$$

Since $\mathbf{n}$ is a vector with entries to be Gaussian i.i.d. and $\mathbf{\Phi}$ is non-overlapped block diagonal with its blocks to be row vectors, $\mathbf{\Phi}\mathbf{n}$ is a vector with entries to be Gaussian independent distributed according to [48].

Considering that the signal in each symbol period has the sparse degree of 1 based on the dictionary $\mathbf{\Psi}$, the decoding part of the symbol contents from the

compressive measurements in this work is developed, motivated by the compressive matched filtering idea in [75]. In compressive matched filtering, with the assumption that the sensing matrix $\mathbf{\Phi}$ is row-wise orthonormal and the phase of the received signal is known to us, the decoding process is done by solving:

$$\min_{\mathbf{x}} \|\mathbf{y} - \mathbf{\Phi}\mathbf{\Psi}\vartheta\|_{l_2}, \text{ s.t. } \|\vartheta\|_{l_0} = 1 \tag{5.4}$$

where $\|\cdot\|_{l_2}$ and $\|\cdot\|_{l_0}$ respectively denote the l_2 and l_0 norms.

In this work, generalized from 5.4, the decoding is started with the Minimum Error (ME) Criterion [76]. In this criterion, decision is made for the choice with the largest posterior probability given the sensed data. Equivalently, we can choose the dictionary atom ψ_k so that for any other dictionary atoms ψ_l, the posterior probability ratio:

$$\Lambda_{k,l} = \frac{Pr(\psi_k|\mathbf{y})}{Pr(\psi_l|\mathbf{y})} \tag{5.5}$$

satisfies $\Lambda_{k,l} \geq 1$, where $Pr(\psi_k|\mathbf{y})$ and $Pr(\psi_l|\mathbf{y})$ respectively denote the posterior probabilities of transmission of the signals corresponding to ψ_k and ψ_l given the measurements $\mathbf{y}$.

The decoded symbol is then decided corresponding to the resulted dictionary atom ψ_k.

5.2.2 Compressive Decoding with Random Measurement Kernels

In most existing literatures, the sensing matrices are chosen to be random. For random sensing matrices, the incoherence requirement between the sensing matrices and the dictionaries can usually be satisfied.

In this work, considering the block-diagonal form of the sensing matrices for the system in Figure 5.1, the non-zero atoms in the random sensing matrices are chosen to be row-wise normalized zero-mean Gaussian.

5.3 Knowledge Enhanced Compressive Decoding of Spread Spectrum Signals

Besides the random sensing matrices discussed above, we also seek for knowledge enhanced compressive coding methods that can improve the decoding accuracy. The knowledge enhanced compressive decoding methods are done based on Linear Discriminant Analysis (LDA) [77, 78].

5.3.1 Decoding Measurement Kernel Design Based on Linear Discriminant Analysis

With the knowledge of the signal structures and the distribution of the dictionary atom usage, we can design the decoding measurement kernels based on LDA. The design process begins with the between-class scatter matrix:

$$\mathbf{R} = \sum_{\substack{k \\ l \neq k}} \varpi_{[k,l]_p} (\mathbf{s}_k - \mathbf{s}_l)(\mathbf{s}_k - \mathbf{s}_l)^H \tag{5.6}$$

where $\mathbf{s}_k$ and $\mathbf{s}_l$ are the k^{th} and l^{th} of the possible signals; and $\varpi_{k,l}$ is the weight for the item $(\mathbf{s}_k - \mathbf{s}_l)(\mathbf{s}_k - \mathbf{s}_l)^H$ in the sum, which is to be determined.

It can be clearly seen that the iterm $(\mathbf{s}_k - \mathbf{s}_l)(\mathbf{s}_k - \mathbf{s}_l)^H$ for every combination of k and l represents the separation of the two possible signals. So as we decide a set of weights $\varpi_{k,l}$'s, we put more or less emphasis on the distinction between some possible signals than others.

After the calculation of the between-class scatter matrix, the measurement kernel is designed according to its principle eigen direction. In fact, according to LDA, the principal eigen direction of the scatter matrix is the optimal projection that separates the different possible signals.

With the knowledge enhanced decoding measurement kernel design method based on LDA as discussed above, we discuss about designing the decoding measurement kernels using the prior distribution of the signals before measurements

are done, and adaptive compressive decoding using the posterior distribution of the signals from previous measurements in the following.

5.3.2 Prior Knowledge Enhanced Compressive Decoding

When designing the prior knowledge enhanced decoding measurement kernel, depending on the dictionary atom positions in the vector space, there are two possible designing methods.

One possible method is to design the entire measurement kernel at once, where the between-class scatter matrix is chosen to be:

$$\mathbf{R} = \sum_{\substack{k \\ l \neq k}} \varpi_{k,l} (\psi_k - \psi_l)(\psi_k - \psi_l)^H \tag{5.7}$$

where ψ_k and ψ_l are chosen to be the k^{th} and the l^{th} columns of the dictionary matrix $\mathbf{\Psi}$ in Equation 5.2, respectively; and the weight parameter $\varpi_{k,l}$ is defined to be the product of the prior probabilities of the signals transmitted corresponding to the k^{th} and the l^{th} columns of the dictionary matrix.

The entire measurement kernel is then chosen to be the principal eigen direction of the scatter matrix. Then the sensing matrix of the compressive decoding during a symbol period is got by fitting the resulted projection vector to the non-zero entries of the sensing matrix during a symbol period.

The other possible method is to design the sensing matrix sequentially for one non-zero row vector block in Figure 3.3 at each time. The design of the non-zero block in the p^{th} $(1 \leq p \leq M)$ row starts with the between-class scatter matrix:

$$\mathbf{R}_p = \sum_{\substack{k \\ l \neq k}} \varpi_{[k,l]_p} (\psi_{k_p} - \psi_{l_p})(\psi_{k_p} - \psi_{l_p})^H \tag{5.8}$$

where the column vector ψ_{k_p} and ψ_{l_p} respectively denote the k^{th} and l^{th} dictionary atoms corresponding to the non-zero block in the p^{th} row of the sensing matrix; and $\varpi_{[k,l]_p}$ denotes the weight to discriminate the vectors ψ_{k_p} and ψ_{l_p}, which is also

the product of the prior probabilities of the signals transmitted corresponding to the k^{th} and l^{th} columns of the dictionary matrix.

Then the non-zero block in the p^{th} row of the sensing matrix is chosen as the normalized principal eigen direction of $\mathbf{R}_p$.

In this way, by designing each of the non-zero blocks, we get the prior knowledge enhanced sensing matrix.

If the dictionary atoms can be clearly separated with projections in some directions, the first method above is implemented. This is straightforward in the sense that the first method finds an optimal measurement space to separate the possibly transmitted signals in this cases. To visually explain this, we take an example to distinguish two classes of signals by a projection, shown in Figure 5.2.

When we project the input signals with the principal eigen direction of the corresponding scatter matrix, which is the optimal linear projection to separate the two classes, the projections will fall on a red line shown in Figure 5.2.

From the sensing matrix aspect, this measurement kernel design strategy based on LDA is equivalent to decomposing the optimal projection of the signals into non-overlapping subspaces. Readers may find that the sensing matrix form of the measurement kernel may not have equal norms for its rows. In fact, the variety of norms for the sensing matrix rows is a kind of weights for the measurements and larger norms suggests a higher importance of the corresponding measurements. On the other hand, by keeping the weights of different measurements, we keep the relationships of all the measurements other than design them independently. An example of two measurements to separate two signal classes is given in Figure 5.3.

In contrast, if the dictionary atoms can not be clearly separated with projections in some directions (e.g. the dictionary atoms uniformly span the vector space), the first method can fail. In this case, we use the second method to design a projection in each single measurement subspace. By collecting the projections from different

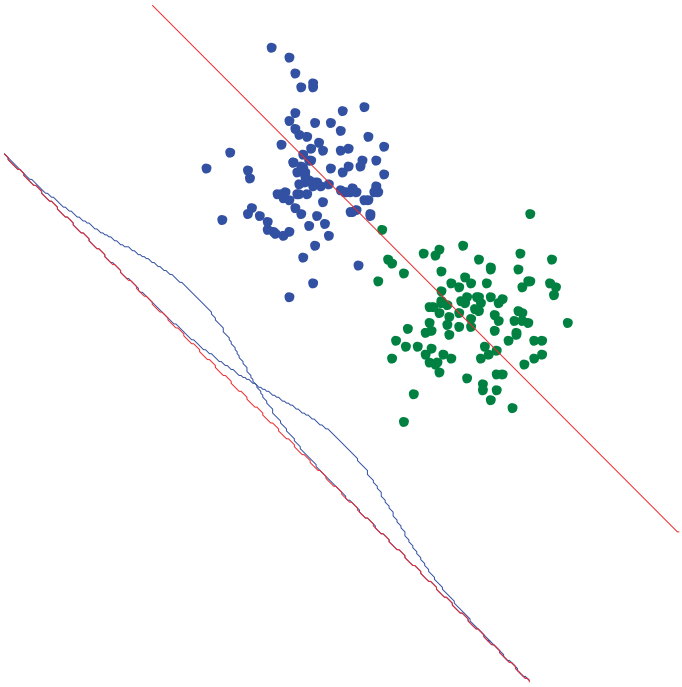

Figure 5.2: Optimal Projection From Principal Eigen Direction of the Scatter Matrix

measurement subspaces, we form the designed measurement kernel and sensing matrix.

5.3.3 Adaptive Compressive Decoding

Our adaptive design starts with a framework, where with a few rows initialized, the measurement kernel in sensing matrix form is designed row by row sequentially. In this framework, each new row is designed based on all of the previous sensed data. When designing the p^{th} row of the sensing matrix (the arbitrary integer $p > 1$ since we need at least one initialized row of the sensing matrix), the scatter matrix

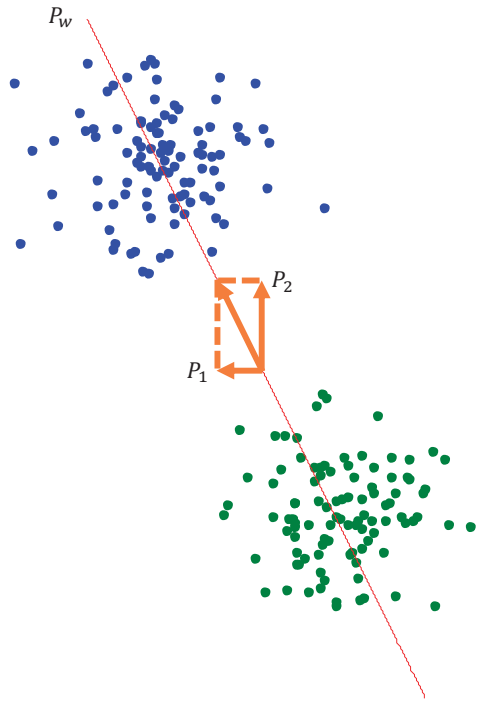

Figure 5.3: Knowledge Enhanced Design of Two Measurements to Separate Two Signal Classes

becomes:

$$\mathbf{R}_p = \sum_{\substack{k \\ l \neq k}} \varpi_{[k,l]_p} (\psi_{k_p} - \psi_{l_p})(\psi_{k_p} - \psi_{l_p})^H \tag{5.9}$$

where ψ_{k_p} and ψ_{l_p} are the respectively the dictionary atoms ψ_k and ψ_l corresponding to the non-zero entries of the p^{th} row in the sensing matrix being designed; and $\varpi_{[k,l]_p}$'s are got based on posterior distribution of the received signals given the measurement $\mathbf{y}_{p-1} = \mathbf{\Phi}_{p-1}(\mathbf{s} + \mathbf{n})$ with the existing $(p-1)$-row sensing matrix $\mathbf{\Phi}_{p-1}$.

The weights $\varpi_{[k,l]_p}$'s in this strategy are calculated by multiplying the posterior probabilities of the possible signals given all of the previous measurements:

$$\varpi_{[k,l]_p} = Pr(\psi_k|\mathbf{y}_{p-1}) Pr(\psi_l|\mathbf{y}_{p-1}) \tag{5.10}$$

With this set-up, we find the non-zero vector block in the p^{th} row of the sensing matrix by taking the normalized principle eigen direction of the scatter matrix calculated by Equation 5.9.

In our work, the initialized rows for the sensing matrix design are chosen as the corresponding rows of the prior knowledge enhanced sensing matrix found in Subsection 5.3.2. As the adaptive compressive decoding proceeds and before we are sure about some dictionary atom (the posterior probability of that dictionary atom after measurements is 1), the conjugate of the new designed rows of the sensing matrix turn out to be more and more correlated to the signal class that is the most probable to be transmitted. On the other hand, this property ensures that the most probable dictionary atom is more and more separated from others.

The block diagram of the sensing part of this adaptive compressive decoding framework is shown in Figure 5.4, where a feedback branch is added from the output to the measurement kernel design block.

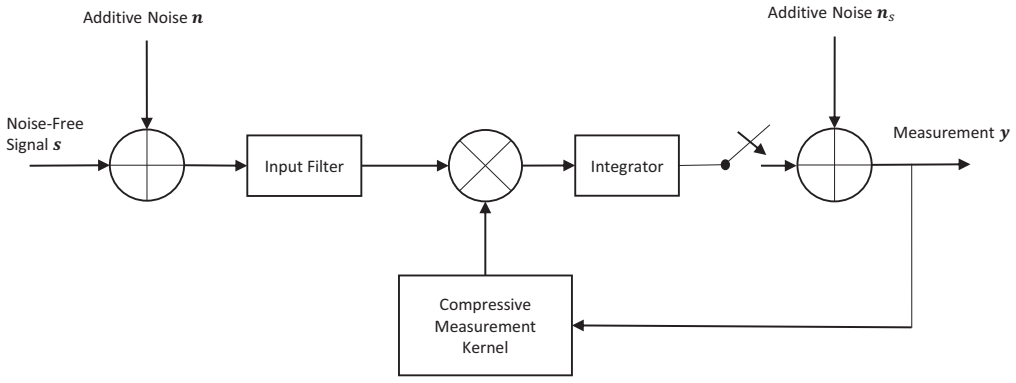

Figure 5.4: Architecture of Ideal Adaptive Compressive Sensing Framework

Great improvement in detectability for this adaptive design is shown in Section 5.7. However, a challenge of the framework exists. The Nyquist interval, the longest period within which a new row of the sensing matrix is designed for this system, is very short, which may make the adaptive sensing matrix design difficult. In the next section, some practical designs to solve the problem based on this framework are proposed.

5.4 Further Improvements of the Decoding System

In this section, we propose two approaches of further improvement in adaptive compressive decoding for our application to solve the problem of the short adaptation time discussed in Subsection 5.3.3. The first approach solves this problem by having more adaptation branches (each adaptation branch includes a feedback branch and a measurement kernel design block) and making them to share the tasks of the framework in Figure 5.4. We call it *Multi-branch Approach* in the following parts. The second approach remains the framework in Figure 5.4, but take idea of the first approach of prior knowledge enhanced measurement kernel design in Subsection 5.3.2. We call it *Multi-fragment Approach* in the following parts. The two approaches are detailed as follows.

5.4.1 Multi-branch Adaptive Measurement Kernel Design Approach

In this subsection, we introduce the multi-branch approach to solve the problem of short adaptation time. In this approach, the total number of adaptation branches, which is also the number of measurement periods cost by an adaptation branch to design a new row of the sensing matrix, is calculated by:

$$N_{br} = \lceil \frac{T_{adp}}{T_{int}} \rceil \tag{5.11}$$

where $\lceil \cdot \rceil$ denotes supremum operation; T_{adp} denotes the time to design a new row of the sensing matrix; and T_{int} denotes the operative period of the switch in Figure

5.4, which is also the time to make a single measurement.

The number of rows to be initialized in the sensing matrix, denoted as N_{ini}, should be at least $N_{br}+1$. Then the other rows of the sensing matrix are designed sequentially with only a single row designed at one time. When designing each row of the sensing matrix, we still consider the nonzero entries of the row in the sensing matrix as we calculate the scatter matrices. However, in his framework, only one in every N_{br} rows is designed by a particular adaptation branch. Moreover, different from the framework discussed in Subsection 5.3.3, we design the p^{th} row based on the 1^{st} through the number $\max\{1, p-N_{br}-1\}$ measurements in this framework; and the weights in Equation 5.10 are calculated with the posterior probability given the corresponding measurements. With the above, all of the adaptation branches cooperate with each other and share a common timeline.

We take the case of $T_{adp} = T_{int} \times 2$ as an example to explain the strategy of the multi-branch framework. In this case, the total number of adaptation branches we need, i.e., N_{br}, is equal to 2 according to Equation 5.11. Assuming that the number of initialized rows, N_{ini}, is equal to $N_{br}+1=3$, and denoting the two adaptation with the letters a and b, respectively, we have the framework of the sensing part of the compressive decoding in Figure 5.5 and the adaptive design process in Table 5.1.

5.4.2 Multi-fragment Adaptive Measurement Kernel Design

In this subsection, we introduce the multi-fragment approach to solve the problem of short adaptation time. In this approach, we remain the framework shown in Figure 5.4 and only have a single adaptive design branch. However, instead of a single row, multiple rows in the sensing matrix are designed at each time. The number of rows to design at one time is:

$$N_{rw} = \min\{N_{ra}, N_{rm}\} \tag{5.12}$$

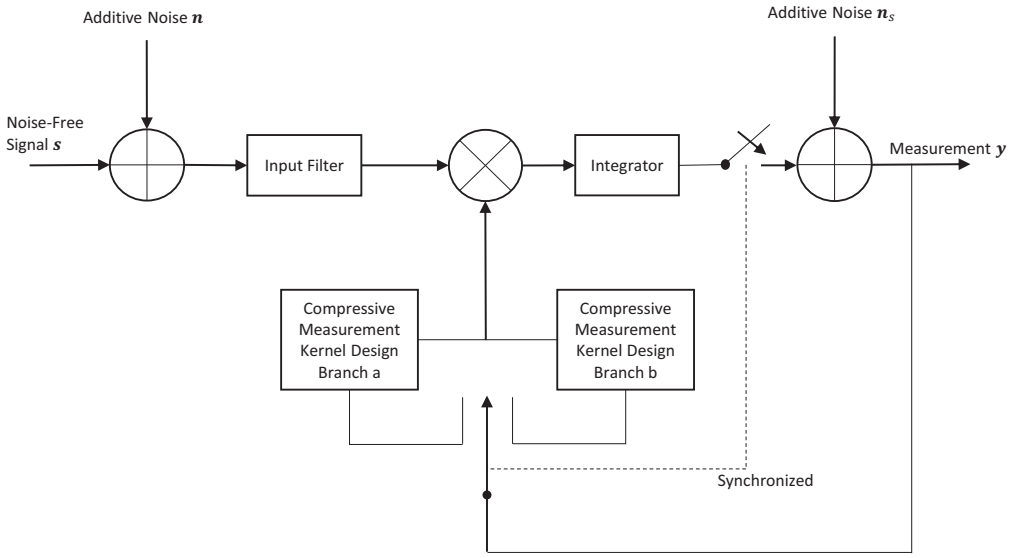

Figure 5.5: Architecture of Multi-branch Adaptive Compressive Sensing Framework with Two Adaptation Branches

where $N_{ra} = \lceil \frac{T_{adp}}{T_{int}} \rceil$ with $\lceil \cdot \rceil$ also to be the number of measurement periods cost for the system to do one adaptation and T_{adp} and T_{int} having the same meaning as Equation 5.11; and N_{rm} denotes the total number of rows remained to design in the sensing matrix.

The number of rows in the sensing matrix needed to be initialized, denoted as N_{ini}, should be at least $N_{ra}+1$, and the p^{th} through the number $p+N_{rw}-1$ rows of the sensing matrix are designed together based on the 1^{st} through the number $p-N_{ra}-1$ measurements, where $p = N_{ini} \times l$ with l to be integer and $p \leq M$.

In this approach, when designing multiple rows (take the p^{th} through the number $p+N_{rw}-1$ rows for example), we take the reference of the first prior knowledge enhanced measurement kernel design method in Subsection 5.3.2 and set the scatter matrix to be:

$$\mathbf{R}_{ps} = \sum_{\substack{k \\ l \neq k}} \varpi_{[k,l]_{ps}} (\psi_{k_{ps}} - \psi_{l_{ps}})(\psi_{k_{ps}} - \psi_{l_{ps}})^H \tag{5.13}$$

Row Being Designed	Adaptation Branch	Measurements Based on
4^{th}	a	1^{st}
5^{th}	b	$1^{st}\rightarrow 2^{nd}$
6^{th}	a	$1^{st}\rightarrow 3^{rd}$
7^{th}	b	$1^{st}\rightarrow 4^{th}$
8^{th}	a	$1^{st}\rightarrow 5^{th}$
9^{th}	b	$1^{st}\rightarrow 6^{th}$
$\vdots$	$\vdots$	$\vdots$

Table 5.1: Example of Adaptive Design with Two Adaptation Branches

where $\psi_{k_{ps}}$ and $\psi_{l_{ps}}$ are respectively the dictionary atoms ψ_k and ψ_l corresponding to where there are the non-zero entries in one of the p^{th} through the number $p+N_{rw}-1$ rows in the sensing matrix to be designed; and $\varpi_{[k,l]_{ps}}$'s are the weights based on posterior distribution of the received signals given the 1^{st} through the number $p-N_{ra}-1$ measurements.

After we find the scatter matrix, we take its normalized principle eigen direction and fit the entries of the vector into the corresponding rows of the sensing matrix.

In this approach, the rows in the sensing matrix designed together are related by the different weights of them, which is similar to the first approach of prior knowledge enhanced measurement kernel design in Subsection 5.3.2. On the other hand, rows designed at different times are related with the adaptations based on the posterior distribution given their previous measurements.

Similar to Subsection 5.4.1, we take the case of $T_{adp} = T_{int} \times 2$ as an example to explain this approach and assume that the number of initialized rows, N_{ini}, is equal to $N_{ra}+1 = 3$. Then the adaptive design process is shown in Table 5.2.

Rows Being Designed	Measurements Based on
$4^{th} \rightarrow 5^{th}$	1^{st}
$6^{th} \rightarrow 7^{th}$	$1^{st} \rightarrow 3^{rd}$
$8^{th} \rightarrow 9^{th}$	$1^{st} \rightarrow 5^{th}$
$\vdots$	$\vdots$

Table 5.2: Example of Adaptive Design with Two Rows of the Sensing Matrix Designed Together

5.5 Compressive Decoding of Frequency-Hopping Spread Spectrum Signals

In this part, we introduce the compressive decoding of FHSS using the proposed systems above. As is introduced in Subsection 2.2.1, the carrier frequency in a FHSS signal hops from time to time. During a hopping period, the frequency domain of the signal is sparse. So decoding based on compressive sensing can be implemented.

In this work, we take the FHSS signal discussed in Subsection 2.2.1. The dictionary in this case is an $N \times (79 \times 4 \times 2)$ ($K = 79 \times 4$) dimensional matrix and is formed as: $\begin{pmatrix} \mathbf{T}_{0,1} & \mathbf{T}_{0,2} & \cdots & \mathbf{T}_{0,79} & \mathbf{T}_{1,1} & \mathbf{T}_{1,2} & \cdots & \mathbf{T}_{1,79} \end{pmatrix}$ with each subblock $\mathbf{T}_{b,i}$ to be $N \times 4$ dimensional. The subblocks with the subscript b represent the cases when symbol b (0 or 1) is transmitted and the subblocks with the subscript i represent the cases when the i^{th} subcarrier is used in the symbol period. Each column of the $\mathbf{T}_{b,i}$ subblock represents a discretized signal in one symbol period with a possible ISI case caused by Gaussian filtering of one of the 4 possible combinations: $[0 \quad b(t) \quad 0]$, $[0 \quad b(t) \quad 1]$, $[1 \quad b(t) \quad 0]$ and $[1 \quad b(t) \quad 1]$. The initial phase of each column in the $\mathbf{T}_{b,i}$ subblock is determined by setting the phase at the beginning of the last symbol period, where the signal in the current symbol period starts to

be influenced in this case, to be zero. Then the sparse representation vector ϑ is a $(4 \times 79 \times 2) \times 1$ binary vector with only 1 entry to be nonzero (i.e. sparsity is 1), which select an dictionary atom.

We note that the waveforms of the noise-free modulated symbols are limited to a number of fixed kinds. It has also been shown in Equation 5.2 that the signals during a symbol period in our sparse representation model are in fact 1-sparse signals based on our dictionary. So the decoding part of the receiver in this application can be modeled as a classifier in Figure 5.6.

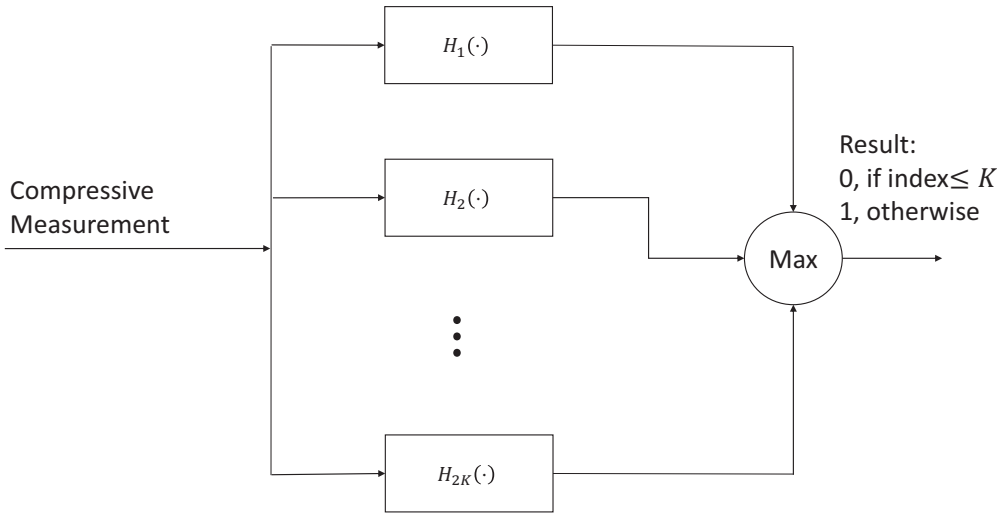

Figure 5.6: Decoding Part of the Receiver

The idea of decoding from compressive measurements is discussed in Section 5.2, where the posterior probabilities of the dictionary atoms $Pr(\psi_j|\mathbf{y})$ are needed. According to the Bayes rule, assuming uniform prior distribution of the dictionary atom usage $\mathbf{s} = \psi_j$ and uniformly distribution of the phase item θ in Equation 2.6 from 0 to 2π, we have:

$$Pr(\psi_j|\mathbf{y}) = \frac{\exp(-\mathbf{y}^H\mathbf{C}_n^{-1}\mathbf{y} - (\mathbf{\Phi}\psi_j)^H\mathbf{C}_n^{-1}(\mathbf{\Phi}\psi_j))\cdot I_0[2|(\mathbf{\Phi}\psi_j)^H\mathbf{C}_n^{-1}\mathbf{y}|]}{\sum_{j=1}^{2K}\exp(-\mathbf{y}^H\mathbf{C}_n^{-1}\mathbf{y} - (\mathbf{\Phi}\psi_j)^H\mathbf{C}_n^{-1}(\mathbf{\Phi}\psi_j))\cdot I_0[2|(\mathbf{\Phi}\psi_j)^H\mathbf{C}_n^{-1}\mathbf{y}|]} \tag{5.14}$$

where $\mathbf{C}_n$ is the covariance matrix (diagonal) of the measured noise $\mathbf{\Phi n}$ and $I_0[\cdot]$ is the zero-ordered modified Bessel function of the first kind.

Details about the derivations of Equation 5.14 are shown in Appendix B.

From Equations 5.5 and 5.14, we get the ratio function:

$$\Lambda_{k,l} = \frac{\exp(-(\mathbf{\Phi}\psi_k)^H \mathbf{C}_n^{-1}(\mathbf{\Phi}\psi_k)) I_0[2|(\mathbf{\Phi}\psi_k)^H \mathbf{C}_n^{-1}\mathbf{y}|]}{\exp(-(\mathbf{\Phi}\psi_l)^H \mathbf{C}_n^{-1}(\mathbf{\Phi}\psi_l)) I_0[2|(\mathbf{\Phi}\psi_l)^H \mathbf{C}_n^{-1}\mathbf{y}|]} \tag{5.15}$$

Then from Equation 5.15, we can establish a set of filters where the j^{th} channel takes the compressive sensed data y as the input and takes

$$F_j(\mathbf{y}) = \exp(-(\mathbf{\Phi}\psi_j)^H \mathbf{C}_n^{-1}(\mathbf{\Phi}\psi_j)) I_0[2|(\mathbf{\Phi}\psi_j)^H \mathbf{C}_n^{-1}\mathbf{y}|] \tag{5.16}$$

as the output. The outputs from different channels are compared to pick the largest one as the corresponding detection choice.

The item $|(\mathbf{\Phi}\psi_j)^H \mathbf{C}_n^{-1}\mathbf{y}|$ in Equation 5.16 is an item of matched filtering and the item $\exp(-(\mathbf{\Phi}\psi_j)^H \mathbf{C}_n^{-1}(\mathbf{\Phi}\psi_\mathbf{j}))$ in Equation 5.16 works as a normalizer. In this case, the filter $H_j(\cdot)$ in Figure 5.6 becomes:

$$H_j(\cdot) = \exp(-(\mathbf{\Phi}\psi_j)^H \mathbf{C}_n^{-1}(\mathbf{\Phi}\psi_j)) I_0[2|\cdot|] \tag{5.17}$$

The dictionary atoms can be separated in the frequency domain, so we adopt the first prior knowledge enhanced sensing matrix design method. More intuitively, we show the relationship of the dictionary items by Multidimensional Scaling (MDS) [79, 80] in Figure 5.7. The MDS is a method to project objects into space with a limited dimension while the divergences between the objects are preserved as well as possible by the distances between the vectors in the projection space. In this work, we take the projection space to be two dimensional and show the relationship of the dictionary atoms in high-dimension space intuitively. In Figure 5.7, we can see that the FHSS dictionary items can be separated clearly by some projections.

The adaptive compressive decoding algorithms discussed in Subsection 5.3.3 and Section 5.4 can be implemented with the posterior distributions calculated with Equation 5.14.

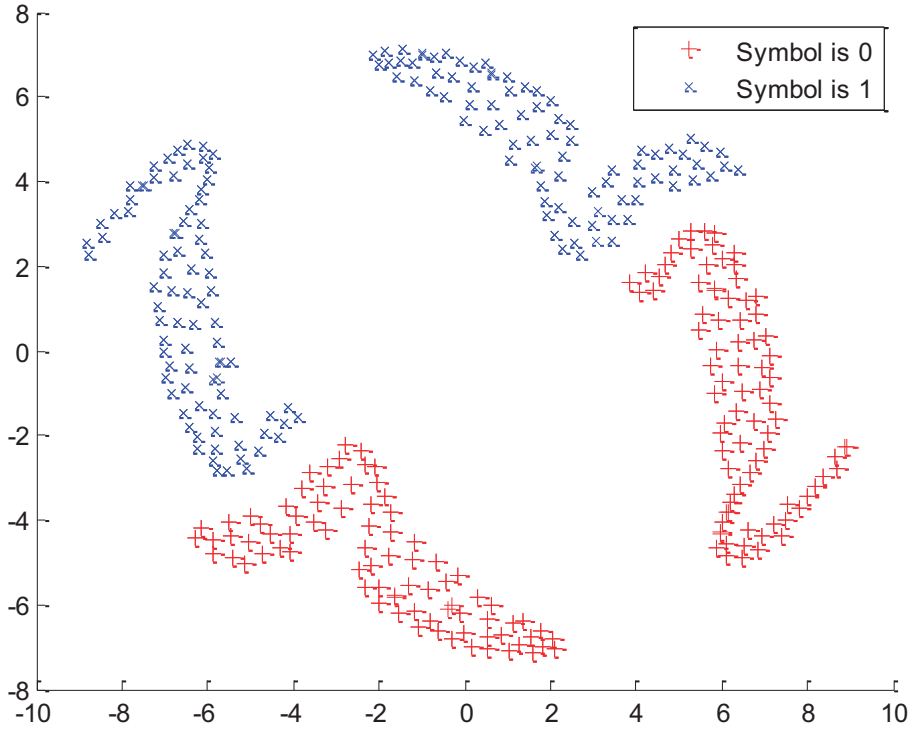

Figure 5.7: MDS of FHSS Dictionary Atoms into 2 Dimensions

The experiment results of the decoding performance in this part are shown in Section 5.7.

5.6 Compressive Decoding of Direct Sequence Spread Spectrum Signals

In this part, we introduce the compressive decoding of DSSS signals using the proposed systems above. As is introduced in Subsection 2.2.2, the DSSS signals spread the spectrum of the signal by modulation with PN sequences. As a result, they appear white in spectra and have much wider bandwidths than the original signals. For SC DSSS sequences, the signal during each symbol period is formed by the modulated symbol content with a PN sequence. With the knowledge of all

the possible PN sequences in use, and denoting that there are in total K candidate PN sequences, the dictionary Ψ is an $N \times 2K$ matrix considering the binary symbol contents. Here N is the number of the Nyquist samples during a symbol period with the Nyquist sampling rate decided by the largest bandwidth spread by the possible PN sequences. Then based on the dictionary, we can get a representation with the sparse degree of 1 for the signal during each symbol period. In this case, decoding based on compressive sensing can be implemented.

In this work, we take the SC DSSS signals with Binary-Shift Phase-Keying (BPSK) modulation discussed in Subsection 2.2.2. as an example of DSSS signals.

The idea of decoding from compressive measurements is discussed in Subsection 5.2.1, where the posterior probabilities of the dictionary atoms $Pr(\psi_j|\mathbf{y})$ are needed. According to the Bayes rule, assuming uniform prior distribution of the dictionary atom usage $\mathbf{s} = \psi_j$, we have:

$$Pr(\psi_j|\mathbf{y}) = \frac{pr(\mathbf{y}|\psi_j)Pr(\psi_j)}{pr(\mathbf{y})} = \frac{pr(\mathbf{y}|\psi_j)Pr(\psi_j)}{\sum_{j=1}^{2K} pr(\mathbf{y}|\psi_j)Pr(\psi_j)} = \frac{pr(\mathbf{y}|\psi_j)}{\sum_{j=1}^{2K} pr(\mathbf{y}|\psi_j)} \tag{5.18}$$

where the likelihood function

$$pr(\mathbf{y}|\psi_j) = \frac{\exp(-(\mathbf{y} - \mathbf{\Phi}\psi_j)^H \mathbf{C}_n^{-1}(\mathbf{y} - \mathbf{\Phi}\psi_j))}{\pi^M \det(\mathbf{C}_n)} \tag{5.19}$$

with $\mathbf{C}_n$ to be the covariance matrix (diagonal) of the measured noise $\mathbf{\Phi n}$.

From Equations 5.18 and 5.19, we have:

$$Pr(\psi_j|\mathbf{y}) = \frac{\exp(-(\mathbf{y} - \mathbf{\Phi}\psi_j)^H \mathbf{C}_n^{-1}(\mathbf{y} - \mathbf{\Phi}\psi_j))}{\sum_{j=1}^{2K} \exp(-(\mathbf{y} - \mathbf{\Phi}\psi_j)^H \mathbf{C}_n^{-1}(\mathbf{y} - \mathbf{\Phi}\psi_j))} \tag{5.20}$$

From Equation 5.5 and 5.20, we get the ratio function:

$$\Lambda_{k,l} = \frac{\exp(2(\mathbf{\Phi}\psi_k)^H \mathbf{C}_n^{-1}\mathbf{y} - (\mathbf{\Phi}\psi_k)^H \mathbf{C}_n^{-1}(\mathbf{\Phi}\psi_k))}{\exp(2(\mathbf{\Phi}\psi_l)^H \mathbf{C}_n^{-1}\mathbf{y} - (\mathbf{\Phi}\psi_l)^H \mathbf{C}_n^{-1}(\mathbf{\Phi}\psi_l))} \tag{5.21}$$

Then from Equation 5.21, and noticing that the exponential function $\exp(\cdot)$ is monotonically increasing, we can establish a set of filters where the j^{th} channel takes the compressive sensed data y as the input and takes

$$F_j(\mathbf{y}) = 2(\mathbf{\Phi}\psi_k)^H \mathbf{C}_n^{-1}\mathbf{y} - (\mathbf{\Phi}\psi_j)^H \mathbf{C}_n^{-1}(\mathbf{\Phi}\psi_j) \tag{5.22}$$

as the output. Then the outputs from different channels are compared to pick the largest one as the corresponding detection choice.

We can see that $2(\mathbf{\Phi}\psi_k)^H\mathbf{C}_n^{-1}\mathbf{y}$ in Equation 5.22 is an item of matched filtering and the item $(\mathbf{\Phi}\psi_j)^H\mathbf{C}_n^{-1}(\mathbf{\Phi}\psi_j)$ works to count for the different effect caused by dictionary atoms.

Then the system in Figure 5.6 can be implemented here, where the filter $H_j(\cdot)$ becomes:

$$H_j(\cdot) = 2(\cdot) - (\mathbf{\Phi}\psi_j)^H\mathbf{C}_n^{-1}(\mathbf{\Phi}\psi_j) \tag{5.23}$$

Because the signals modulated by PN sequences uniformly span the signal space, the dictionary atoms can not be separated, we adopt the second prior knowledge enhanced sensing matrix design method. More intuitively, the relationship of the dictionary items can be shown by MDS in Figure 5.8, where dictionary items can not be separated by any particular projections.

The adaptive compressive decoding algorithm discussed in Subsection 5.3.3 and Section 5.4 can be implemented with the posterior distributions calculated with Equations 5.18.

The experiment results of the decoding performance in this part are also shown in Section 5.7.

5.7 Experimental Results

5.7.1 Compressive Decoding of Frequency-Hopping Spread Spectrum Signals

In this subsection, we show the compressive decoding simulation results of FHSS signals. The FHSS signals used in these experiments are specified in Subsection 2.2.1 and we discuss the simulation results on different CRs and SNRs at the receiver to verify our proposed compressive decoding approaches for the FHSS

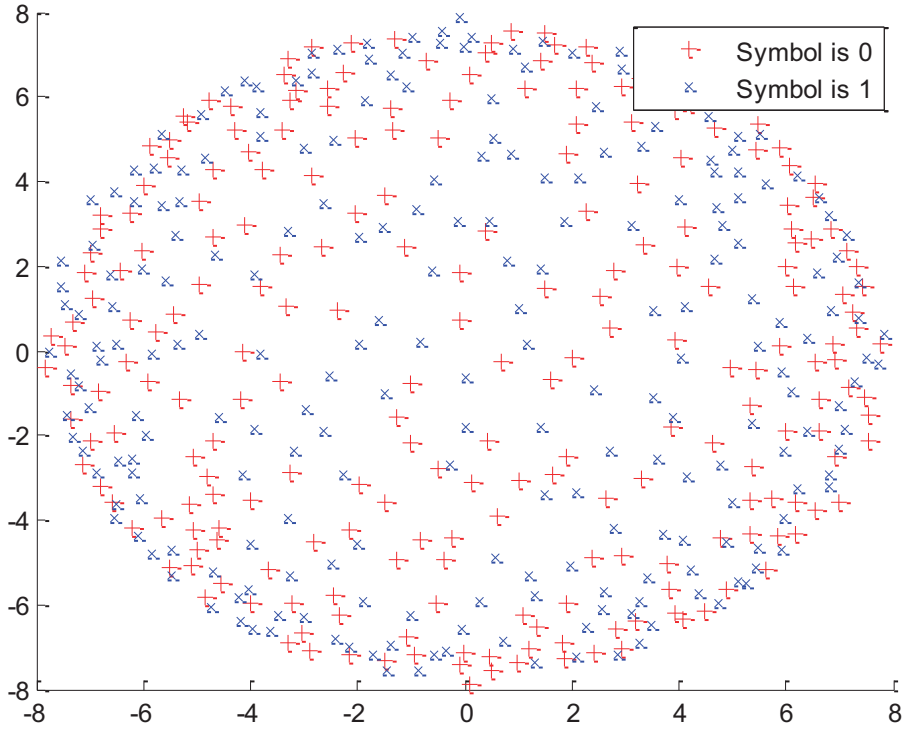

Figure 5.8: MDS of DSSS Dictionary Atoms into 2 Dimensions

signals.

Firstly, we compare the compressive decoding approaches of FHSS signals in Section 5.5. Simulations were done for the input discretizing rate in our DD system model to be twice of the frequency hopping range. The CR, defined by the ratio between the Nyquist rate with respect to the entire FHSS hopping range and the compressive measurement rate varied from 5 to 15; and the SNR at the receiver varied from $0dB$ to $30dB$. When doing the ideal adaptive compressive decoding, which assumed the short adaptation time, the first row of the sensing matrix was initialized with that in the prior knowledge enhanced sensing matrix assuming uniform prior of the dictionary atoms. The results are shown in Figure 5.9. For comparison, we also have the simulation results of the ideal non-compressed case plotted.

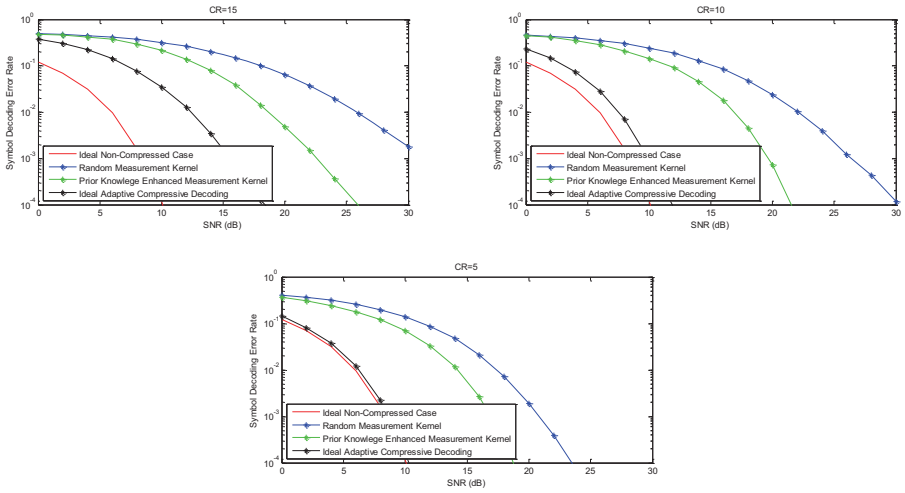

Figure 5.9: Comparison of Symbol Detection Error Rate versus SNR at the Receiver for Different Sensing Matrix Design Approaches of FHSS Signals

It can be seen that among compressed approaches in Figure 5.9, the compressive decoding with random sensing matrices has good decoding performance, while saving a lot of hardware cost. With knowledge enhanced approaches, we get improvement from the decoding with randomsensing matrices: The prior knowledge enhanced measurement kernel performs apparently better than the random matrix and this improvement can be several orders in magnitude of reduction of decoding error rate at the same SNR or several dB reduction to achieve the same decoding accuracy. The ideal adaptive compressive decoding approach has the best performance in the decoding task. Especially when the compression ratio is not too high, the decoding error rate is very close to the ideal non-compressed case.

Then, we show the simulation results to see the performance of the multi-branch realization of the adaptive compressive decoding. We still took the input discretizing rate in our DD system model to be twice of the frequency hopping range, varied the CR from 5 to 15 and the SNR at the receiver from $0dB$ to $30dB$, and varied the number of measurement intervals cost by each adaptive design of each adaptation branch. For each adaptive design time case, we had the minimum

number of initialized rows for the sensing matrix drawn from the prior knowledge enhanced sensing matrix assuming uniform prior of the dictionary atoms for each adaptive design time case. The simulation results are shown in Figure 5.10. For comparison, we also have the simulation results of the ideal non-compressed cases, the random sensing matrices case, the prior knowledge enhanced sensing matrices case and the ideal adaptive compressive decoding case plotted.

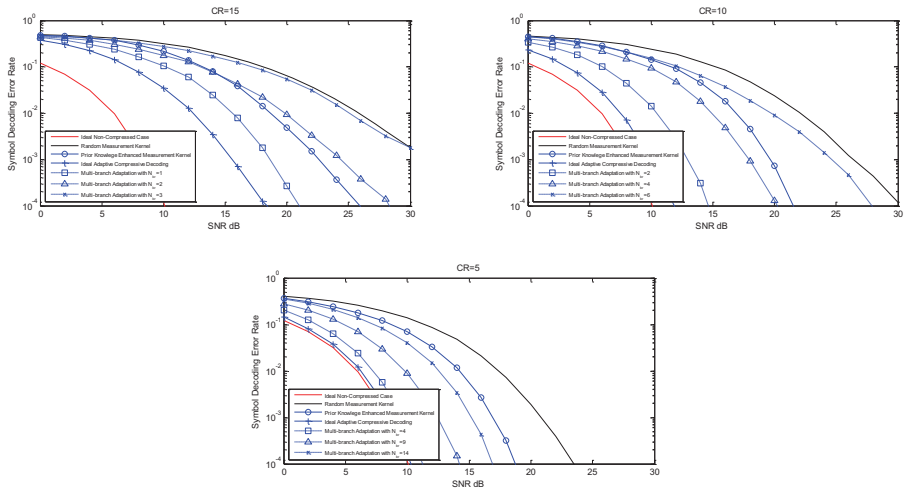

Figure 5.10: Comparison of Symbol Detection Error Rate versus SNR at the Receiver for Multi-branch Compressive Decoding Realization and Other Design Approaches of FHSS Signals

It can be seen that among the compressive decoding approaches in Figure 5.10, the ideal adaptive compressive decoding approach, which assumes the shortest time for adaptation design, has the best performance in decoding. The more adaptation design time we use for each adaptation design row, the worse the decoding performance we have. This performance can be even worse than the prior knowledge enhanced approach when the adaptation time is very long. This is because for longer adaptive design time case, the information we get from the previous measurements is not "new" enough comparing to the cases when we have shorter adaptive design time. The implementation of these out-of-date information for very long adaptation times can even lead to worse results than just using the prior

knowledge.

Finally, we show simulation results to see the performance of the multi-fragment realization of the adaptive compressive sensing. The same input discretizing rate in the DD system model, CRs and SNRs at the receivers were used for the FHSS in this experiment. We varied the number of measurement intervals cost by each adaptive design of the adaptive design branch. Similar to the multi-branch adaptive compressive sensing simulations, we had the minimum number of initialized rows for the sensing matrix drawn from the prior knowledge enhanced sensing matrix for each adaptive design time case. The simulation results are shown in Figure 5.11. For comparison, we also have the simulation results of the ideal non-compressed case, the random sensing matrices case, the prior knowledge enhanced sensing matrices case and the ideal adaptive compressive decoding case plotted.

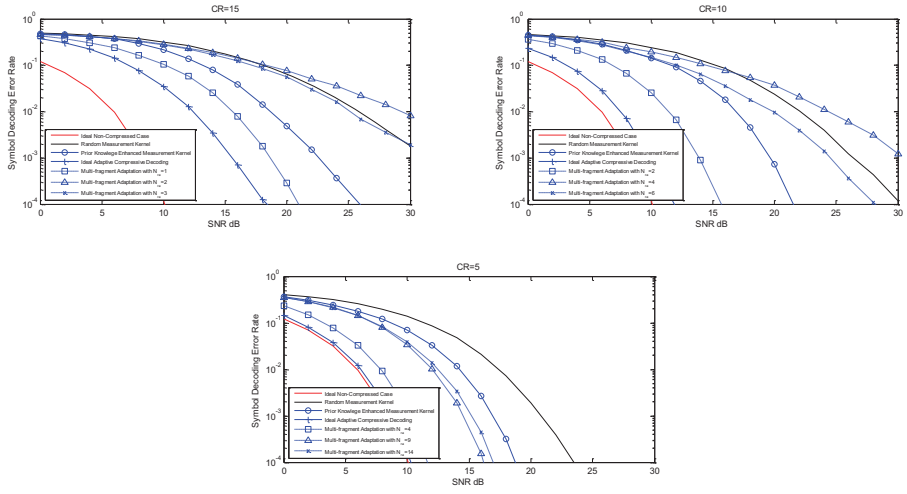

Figure 5.11: Comparison of Symbol Detection Error Rate versus SNR at the Receiver for Multi-fragment Compressive Sensing Realization and Previous Design Approaches of FHSS Signals

From Figure 5.11, similar to the multi-branch adaptive compressive sensing simulation results, we can also see that among the adaptive approaches in Figure 5.11, the ideal adaptive compressive decoding approach, which assumes the shortest time

for adaptive design, has the best performance in decoding. For short adaptation time cases, the more adaptation design time we use in adaptive design for each time, the worse the decoding performance we have. This performance can be even worse than the prior knowledge enhanced approach for very long adaptation times. However, when the adaption time is longer than some value, the multi-branch adaptive compressive sensing performance starts to improve and finally converges to the prior knowledge enhance case. One additional observation we get from this part is that since the multi-fragment adaptive compressive decoding method involve less hardware than multi-branch, the multi-fragment method has worse decoding performance than the multi-branch method with the same amount of adaptive design time at each time, which is a trade-off in this case.

5.7.2 Compressive Decoding of Direct Sequence Spread Spectrum Signals

We then show the compressive decoding simulation results of DSSS signals in this subsection. The DSSS signals used in these experiments are specified in Subsection 2.2.2 and we discuss the simulation results on different CRs and SNRs at the receiver to verify our proposed compressive decoding approaches for the DSSS signals.

Similar to the FHSS experiments, we firstly compare the compressive decoding approaches of DSSS signals in Section 5.6. Simulations were done for the input discretizing rate in our DD system model to be Nyquist sampling rate of the signals modulated with the highest possible ordered m-sequence. The CR, defined by the ratio between the Nyquist rate with respect to the Nyquist sampling rate of the signals modulated with the highest possible ordered m-sequence and the compressive measurement rate varied from 2 to 5; and the SNR at the receiver varied from $-10dB$ to $20dB$. When doing the ideal adaptive compressive decoding, which assumed the short adaptation time, the first row of the sensing matrix was initialized with the knowledge enhanced sensing matrix. The results are shown

in Figure 5.12. For comparison, we also have the simulation results of the ideal non-compressed case plotted.

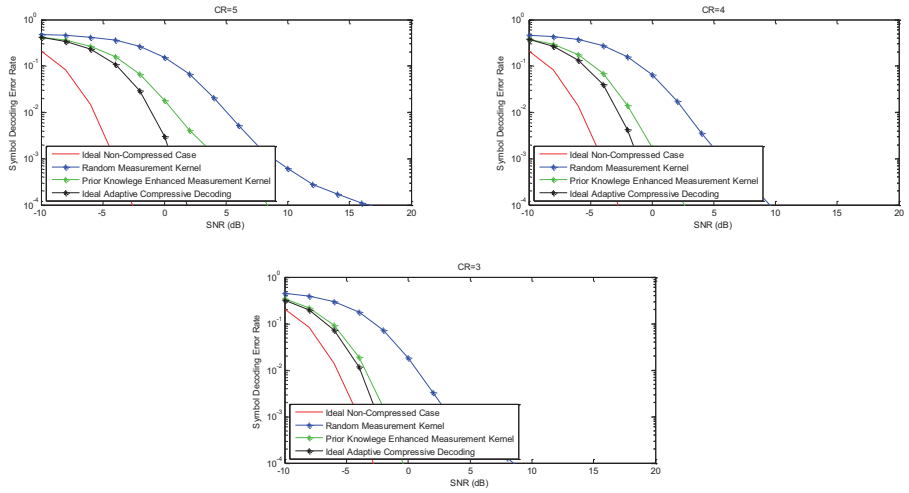

Figure 5.12: Comparison of Symbol Detection Error Rate versus SNR at the Receiver for Different Sensing Matrix Design Approaches of DSSS Signals

Similar to the FHSS case, we find that the compressive decoding with random sensing matrices has good decoding performance, while saving a lot in the harware cost. With knowledge enhanced decoding methods, we can get several orders of magnitude reduction in the decoding error rate at some SNR values or several dB reduction to achieve the same decoding accuracy. The prior knowledge enhanced measurement kernel performs apparently better than the random matrix and the ideal adaptive compressive decoding approach has the best performance in the decoding task.

We then show the simulation results to see the performance of the multi-branch realization of the adaptive compressive decoding. We still took the input discretizing rate in our DD system model to be Nyquist sampling rate of the signals modulated with the highest possible ordered m-sequence, varied the CR from 3 to 5 and the SNR at the receiver from $-10dB$ to $20dB$, and varied the number of measurement intervals cost by each adaptive design of each adaptation branch. For

each adaptive design time case, we had the minimum number of initialized rows for the sensing matrix drawn from the prior knowledge enhanced sensing matrix in Subsection for each adaptive design time case. The simulation results are shown in Figure 5.13. For comparison, we also have the simulation results of the ideal non-compressed cases, the random sensing matrices case, the prior knowledge enhanced sensing matrices case and the ideal adaptive compressive decoding case plotted.

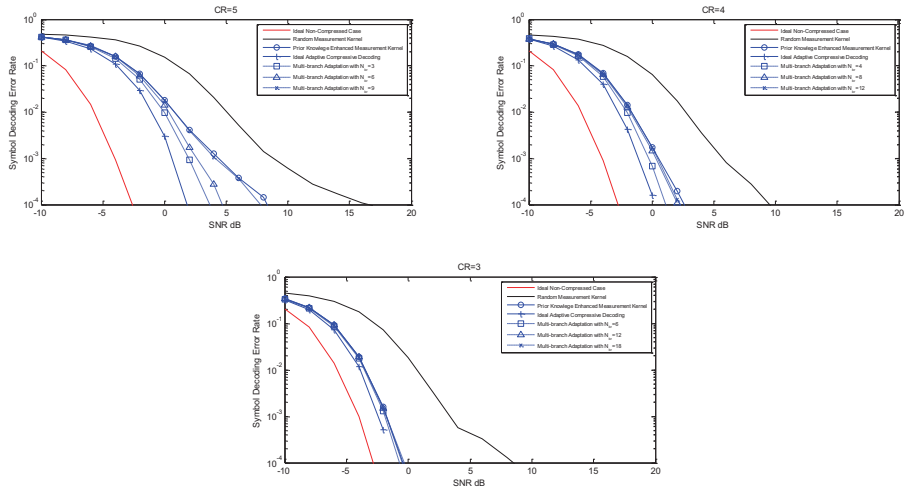

Figure 5.13: Comparison of Symbol Detection Error Rate versus SNR at the Receiver for Multi-branch Compressive Decoding Realization and Other Design Approaches of DSSS Signals

Similar to the FHSS case, it can be seen that among the compressive decoding approaches in Figure 5.13, the ideal adaptive compressive decoding approach, which assumes the shortest time for adaptation design, has the best performance in decoding. The more adaptation design time we use for each adaptation design row, the worse the decoding performance we have. In the DSSS case, it is espectially obvious for high compression ratio cases.

Finally, we show simulation results to see the performance of the multi-fragment realization of the adaptive compressive sensing. The same input discretizing rate in the DD system model, CRs and SNRs at the receivers were used for the DSSS

in this experiment. We varied the number of measurement intervals cost by each adaptive design of the adaptive design branch. Similar to the multi-branch adaptive compressive sensing simulations, we had the minimum number of initialized rows for the sensing matrix drawn from the prior knowledge enhanced sensing matrix for each adaptive design time case. The simulation results are shown in Figure 5.14. For comparison, we also have the simulation results of the ideal non-compressed case, the random sensing matrices case, the prior knowledge enhanced sensing matrices case and the ideal adaptive compressive decoding case plotted.

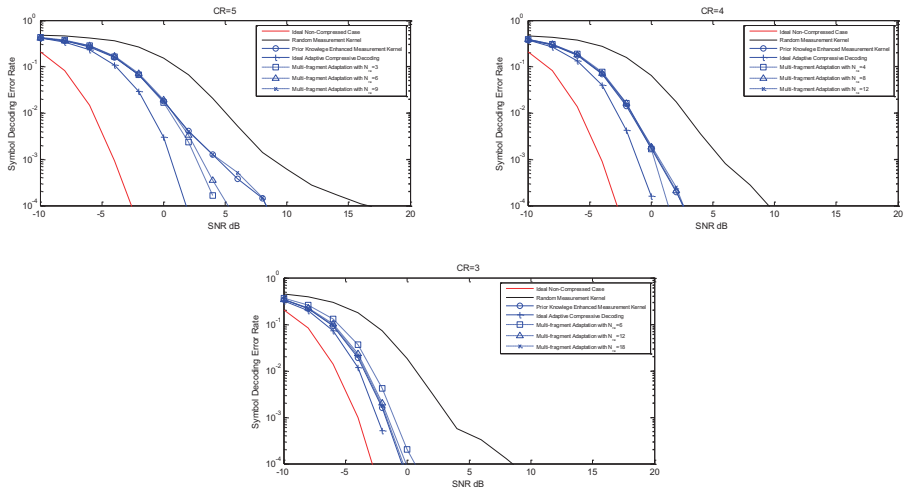

Figure 5.14: Comparison of Symbol Detection Error Rate versus SNR at the Receiver for Multi-fragment Compressive Sensing Realization and Previous Design Approaches of DSSS Signals

From Figure 5.14, similar to the multi-branch adaptive compressive sensing simulation results, we can also see that among the adaptive approaches in Figure 5.14, the ideal adaptive compressive decoding approach, which assumes the shortest time for adaptive design, has the best performance in decoding. The more adaptation design time we use in adaptive design for each time, the worse the decoding performance we have. The performance can be even worse than the prior knowledge enhance method for very long adaptation times and if the adaption time keeps increasing, the decoding performance finally converges to the prior knowledge

enhance case. Also similar to the FHSS case, with the same amount of adaptive design time at each time, the multi-fragment method has worse decoding performance than the multi-branch method, as the multi-fragment adaptive compressive decoding method involve less hardware than multi-branch, which is a trade-off.

5.8 Conclusion

With the presence detection of the SS signals using the compressive detection approaches proposed in Chapter 3 and Chapter 4, we proposed the non-cooperative compressive decoding approaches of SS signals. Besides the compressive decoding approach with random measurement kernels, by observing the structure and distribution of the signals, we also proposed knowledge enhanced compressive decoding approaches based on LDA. With the prior knowledge of the signal distribution and posterior knowledge of the signal distribution based on the previous measurements, we respectively proposed prior knowledge enhanced and adaptive compressive decoding approaches. Moreover, two approaches to modify the adaptive compressive decoding system are proposed to allow more time for the adaptive hardware to design the measurement kernels.

The proposed compressive decoding approaches were implemented to the FHSS signals and DSSS signals discussed in Section 2.2 as examples of SS signals. We showed that he compressive decoding approaches operate at much lower sampling rate than the Nyquist rate with respect to the entire SS spread spectrum while still with good decoding accuracy performance. We also showed that by implementing knowledge enhanced compressive decoding approaches, improved decoding accuracy performance over that with random measurement kernels could be achieved.

CHAPTER 6

CONCLUSIONS

In this dissertation, we presented several novel approaches for compressive sensing of spread spectrum signals. In Chapter 3, we introduced methods for non-cooperative compressive detection of FHSS signals. We first introduced a compressive detection approach that used random measurement kernels. We then introduced a compressive detection system with designed measurement kernels where the measurement kernels were designed using an information theoretic metric called Task-Specific Information. Finally, we illustrated how the measurement kernels could be adapted during the measurement process. The results obtained in this section illustrated that compressive detection methods did not suffer from the FNR "floor" problem which was observed in conventional scanning systems when the relative the scanning rate was low and the SNR was high. Experiments also illustrated that the designed measurement kernels could achieve superior detection performance compared to random measurement kernels. In Chapter 4, we introduced methods for non-cooperative compressive detection of DSSS signals. We considered two conventional DSSS detection approaches; one based on energy and another one based on autocorrelation. We proposed compressive implementations for both approaches using random measurement kernels. We then extended our discussion to designed measurement kernels and proposed prior-knowledge enhanced measurement kernels and adaptive measurement kernels for both systems. Results presented in Chapter 4 illustrated that the compressive systems, while operating at reduced sampling rates, achieved competitive performance. In particular, the energy-based adaptive compressive detection system outperformed its non-compressive counterpart. The goal of the systems discussed in Chapters 3 and 4 was to detect the presence of spread spectrum signals. In contrast, we proposed methods for non-cooperative compressive decoding of spread spectrum signals in

Chapter 5. The goal of these methods was to recover the symbols from compressive measurements. Both FHSS and DSSS signals were considered in this chapter. Similar to previous chapters, we introduced methods that utilized both random and designed measurement kernels. Both prior knowledge enhanced and adaptive compressive decoding approaches were introduced. In addition, several adaptation methods that provided a trade-off between decoding performance and hardware constraints were discussed.

APPENDIX A

DERIVATION OF THE TASK-SPECIFIC INFORMATION GRADIENT BASED ON MIXTURE OF GAUSSIAN MODEL IN FHSS SIGNAL DETECTION

In this part, we provide the details in the derivations of Equation (3.31), Equation (3.32) and Equation (3.33).

If we model the input signal without noise as mixture of Gaussian as specified in Equation (3.30), and the additive noise as zero-mean Gaussian white over the entire FHSS hopping range with the variance σ_n^2, then the distribution of the m^{th} measurement during the i^{th} observation interval $\mathbf{y}_{i,m}$ is also a mixture of Gaussian:

$$f(\mathbf{y}_{i,m}) = P_s \sum_{l=1}^{L} P_l f_l(\mathbf{y}_{i,m}) + (1 - P_s) f_0(\mathbf{y}_{i,m}) \tag{A.1}$$

where P_s denotes the probability of signal present;

$$f_0(\mathbf{y}_{i,m}) = CN(\mathbf{0}, \sigma_n^2 \mathbf{\Phi}_{i,m} \mathbf{I}_{CR} \mathbf{\Phi}_{i,m}^{\dagger}) \tag{A.2}$$

denotes the distribution of $\mathbf{y}_{i,m}$ in the case of signal absent; and

$$f_l(\mathbf{y}_{i,m}) = CN(\mathbf{0}, \mathbf{\Phi}_{i,m} \mathbf{C}_{xx}^{(l)} \mathbf{\Phi}_{i,m}^{\dagger}) \tag{A.3}$$

with $\mathbf{C}_{xx}^{(l)} = \mathbf{C}_{ss}^{(l)} + \sigma_n^2 \mathbf{I}_{CR}$, and $\mathbf{I}_{CR}$ to be the $CR \times CR$ identity matrix.

Then we have

$$\begin{aligned} & H(\mathbf{y}_{i,m}) \\ & = -\int f(\mathbf{y}_{i,m}) \log[f(\mathbf{y}_{i,m})] d\mathbf{y}_{i,m} \\ & = -\int (P_s \sum_{l=1}^{L} P_l f_l(\mathbf{y}_{i,m}) + (1 - P_s) f_0(\mathbf{y}_{i,m})) \\ & \cdot \log[P_s \sum_{l=1}^{L} P_l f_l(\mathbf{y}_{i,m}) + (1 - P_s) f_0(\mathbf{y}_{i,m})] d\mathbf{y}_{i,m} \end{aligned} \tag{A.4}$$

If we do Taylor extension of $\log[P_s \sum_{l=1}^{L} P_l f_l(\mathbf{y}_{i,m}) + (1-P_s) f_0(\mathbf{y}_{i,m})]$ at $E[\mathbf{y}_{i,m}] = \mathbf{0}$, we get:

$$\begin{aligned}
&\log[P_s \sum_{l=1}^{L} P_l f_l(\mathbf{y}_{i,m}) + (1-P_s) f_0(\mathbf{y}_{i,m})] \\
&= \log[P_s \sum_{l=1}^{L} P_l f_l(\mathbf{0}) + (1-P_s) f_0(\mathbf{0})] + \\
&\nabla_{\mathbf{y}_{i,m}} \{\log[P_s \sum_{l=1}^{L} P_l f_l(\mathbf{y}_{i,m}) + (1-P_s) f_0(\mathbf{y}_{i,m})]\}|_{\mathbf{y}_{i,m}=\mathbf{0}} \\
&\cdot \mathbf{y}_{i,m} + \dots \\
&\approx \log[P_s \sum_{l=1}^{L} P_l f_l(\mathbf{0}) + (1-P_s) f_0(\mathbf{0})] + G(\mathbf{0}) \cdot \mathbf{y}_{i,m}
\end{aligned} \tag{A.5}$$

Substituting Equation (A.5) into Equation (A.4), we get:

$$\begin{aligned}
&H(\mathbf{y}_{i,m}) \\
&\approx -\int (P_s \sum_{l=1}^{L} P_l f_l(\mathbf{y}_{i,m}) + (1-P_s) f_0(\mathbf{y}_{i,m})) \\
&[\log[P_s \sum_{l=1}^{L} P_l f_l(\mathbf{0}) + (1-P_s) f_0(\mathbf{0})] + G(\mathbf{0}) \cdot \mathbf{y}_{i,m}] d\mathbf{y}_{i,m} \\
&= -\log[P_s \sum_{l=1}^{L} P_l f_l(\mathbf{0}) + (1-P_s) f_0(\mathbf{0})] \\
&= -\log[P_s \sum_{l=1}^{L} \frac{P_l}{\pi^M |\mathbf{\Phi}_{i,m} \mathbf{C}_{xx}^{(l)} \mathbf{\Phi}_{i,m}^{\dagger}|} + \frac{1-P_s}{\pi^M |\sigma_n^2 \mathbf{\Phi}_{i,m} \mathbf{I}_{CR} \mathbf{\Phi}_{i,m}^{\dagger}|}]
\end{aligned} \tag{A.6}$$

where $|\cdot|$ denotes the determinant operator.

Similarly, since the conditional distribution of $\mathbf{y}_{i,m}$ given $\mathbf{s}_{i,m}$ is:

$$f(\mathbf{y}_{i,m}|\mathbf{s}_{i,m}) = CN(\mathbf{s}_{i,m}, \sigma_n^2 \mathbf{\Phi}_{i,m} \mathbf{I}_{CR} \mathbf{\Phi}_{i,m}^{\dagger}) \tag{A.7}$$

and the entropy of $\mathbf{y}_{i,m}$ conditional on $\mathbf{s}_{i,m}$ is calculated by:

$$H(\mathbf{y}_{i,m}|\mathbf{s}_{i,m}) \approx -\log[\frac{1}{\pi^M |\sigma_n^2 \mathbf{\Phi}_{i,m} \mathbf{I}_{CR} \mathbf{\Phi}_{i,m}^{\dagger}|}] \tag{A.8}$$

the entropy of $\mathbf{y}_{i,m}$ in the signal presence case is calculated by:

$$H(\mathbf{y}_{i,m}|\text{signal present}) \approx -\log[\sum_{l=1}^{L} \frac{P_l}{\pi^M |\mathbf{\Phi}_{i,m}\mathbf{C}_{xx}^{(l)}\mathbf{\Phi}_{i,m}^{\dagger}|}] \tag{A.9}$$

From Equation (A.6) and Equation (A.8), we can get:

$$\begin{aligned} & I(\mathbf{y}_{i,m};\mathbf{s}_{i,m}) \\ & \approx -\log[P_s \sum_{l=1}^{L} \frac{P_l}{\pi^M |\mathbf{\Phi}_{i,m}\mathbf{C}_{xx}^{(l)}\mathbf{\Phi}_{i,m}^{\dagger}|} + \frac{1-P_s}{\pi^M |\sigma_n^2 \mathbf{\Phi}_{i,m}\mathbf{I}_{CR}\mathbf{\Phi}_{i,m}^{\dagger}|}] \\ & + \log[\frac{1}{\pi^M |\sigma_n^2 \mathbf{\Phi}_{i,m}\mathbf{I}_{CR}\mathbf{\Phi}_{i,m}^{\dagger}|}] \end{aligned} \tag{A.10}$$

If $\mathbf{\Phi}_{i,m}$ is normalized, then from Equation (A.9) and Equation (A.10), Equation (3.25) and Equation (3.26) can be substituted with Equation (3.31) and Equation (3.32).

Using the chain rule for the derivatives, we get:

$$\begin{aligned} & \nabla_{\mathbf{\Phi}_{i,m}} H(\mathbf{y}_{i,m}|\text{signal present}) \\ & \approx \nabla_{\mathbf{\Phi}_{i,m}} \{-\log[\sum_{l=1}^{L} \frac{P_l}{\pi^M |\mathbf{\Phi}_{i,m}\mathbf{C}_{xx}^{(l)}\mathbf{\Phi}_{i,m}^{\dagger}|}]\} \\ & = -\frac{\sum_{l=1}^{L} P_l \pi^{-M} \nabla_{\mathbf{\Phi_{i,m}}} \{|\mathbf{\Phi}_{i,m}\mathbf{C}_{xx}^{(l)}\mathbf{\Phi}_{i,m}^{\dagger}|^{-1}\}}{\sum_{l=1}^{L} P_l \pi^{-M} |\mathbf{\Phi}_{i,m}\mathbf{C}_{xx}^{(l)}\mathbf{\Phi}_{i,m}^{\dagger}|^{-1}} \\ & = \frac{\sum_{l=1}^{L} P_l \pi^{-M} |\mathbf{\Phi}_{i,m}\mathbf{C}_{xx}^{(l)}\mathbf{\Phi}_{i,m}^{\dagger}|^{-1} (\mathbf{\Phi}_{i,m}\mathbf{C}_{xx}^{(l)}\mathbf{\Phi}_{i,m}^{\dagger})^{-1} \mathbf{\Phi}_{i,m}\mathbf{C}_{xx}^{(l)\dagger}}{\sum_{l=1}^{L} P_l \pi^{-M} |\mathbf{\Phi}_{i,m}\mathbf{C}_{xx}^{(l)}\mathbf{\Phi}_{i,m}^{\dagger}|^{-1}} \\ & = \frac{\sum_{l=1}^{L} P_l |\mathbf{\Phi}_{i,m}\mathbf{C}_{xx}^{(l)}\mathbf{\Phi}_{i,m}^{\dagger}|^{-1} (\mathbf{\Phi}_{i,m}\mathbf{C}_{xx}^{(l)}\mathbf{\Phi}_{i,m}^{\dagger})^{-1} \mathbf{\Phi}_{i,m}\mathbf{C}_{xx}^{(l)\dagger}}{\sum_{l=1}^{L} P_l |\mathbf{\Phi}_{i,m}\mathbf{C}_{xx}^{(l)}\mathbf{\Phi}_{i,m}^{\dagger}|^{-1}} \end{aligned} \tag{A.11}$$

APPENDIX B

DERIVATION OF COMPRESSIVE MATCHED FILTER FOR FHSS SIGNALS

In this part, we detail the derivations of the posterior distribution of dictionary atom usage given the measurement vectors for FHSS signals.

We note that without regards of the influence by the phase, the waveforms of the noiseless modulated symbols are limited to a number of fixed kinds. It has also been shown in Equation 5.2 that the Bluetooth signals during a symbol period in our sparse representation model are in fact 1-sparse signals based on our dictionary.

The main challenge in our design of the compressive matched filter in the practical Bluetooth signal is the initial phase at the beginning of one symbol period caused by the initialized random phase at the beginning of the sequence and the accumulated phase from the previous symbol periods. In this case, Equation 5.4 becomes:

$$\min_{\mathbf{x}} \|\mathbf{y}\exp(i\theta) - \mathbf{\Phi\Psi x}\|_{l_2} \tag{B.1}$$

where θ is the random phase mentioned above.

We solve this problem with the reference to ME criterion, which has been discussed in Section 5.2 and we need to firstly need to find the posterior distribution of the dictionary atom usage give the measurements.

According to the Bayes rule, the posterior distribution of the dictionary atom usage give the measurement is given by:

$$Pr(\psi_j|\mathbf{y}) = \frac{pr(\mathbf{y}|\psi_j)Pr(\psi_j)}{pr(\mathbf{y})} = \frac{pr(\mathbf{y}|\psi_j)Pr(\psi_j)}{\sum_{j=1}^{4\times 79\times 2} pr(\mathbf{y}|\psi_j)Pr(\psi_j)} \tag{B.2}$$

We assume uniform prior distribution of the signals $\mathbf{s} = \psi_j$, for $j = 1, 2, \cdots, 4\times$

79×2, then Equation B.2 becomes

$$Pr(\psi_j|\mathbf{y}) = \frac{pr(\mathbf{y}|\psi_j)}{\sum_{j=1}^{4\times 79\times 2} pr(\mathbf{y}|\psi_j)} \tag{B.3}$$

We also assume that the phase item θ is uniformly distributed form 0 to 2π, then the conditional probability density in Equation B.3 becomes:

$$pr(\mathbf{y}|\psi_j) = \int_0^{2\pi} pr(\mathbf{y}|\psi_j, \theta) pr(\theta) d\theta = \frac{1}{2\pi} \int_0^{2\pi} pr(\mathbf{y}|\psi_j, \theta) d\theta \tag{B.4}$$

From Equation 5.3, we note that given the phase θ, the entries of $\mathbf{y}$ are Gaussian independent distributed with their correponding mean values to be the entries of the vector $\mathbf{\Phi s}$. Then we have:

$$pr(\mathbf{y}|\psi_j, \theta) = \frac{1}{\pi^M \det(\mathbf{C}_n)} \cdot \exp(-(\mathbf{y} - \exp(i\theta)\mathbf{\Phi}\psi_j)^H \mathbf{C}_n^{-1} (\mathbf{y} - \exp(i\theta)\mathbf{\Phi}\psi_j)) \tag{B.5}$$

where $\mathbf{C}_n$ is the covariance matrix (diagonal) of the measured noise $\mathbf{\Phi n}$.

From Equation B.4 and Equation B.5, we have:

$$pr(\mathbf{y}|\psi_j) = \frac{\exp(-\mathbf{y}_H \mathbf{C}_n^{-1} \mathbf{y} - (\mathbf{\Phi}\psi_j)^H \mathbf{C}_n^{-1} (\mathbf{\Phi}\psi_j))}{\pi^M \det(\mathbf{C}_n)} \cdot I_0[2|(\mathbf{\Phi}\psi_j)^H \mathbf{C}_n^{-1} \mathbf{y}|] \tag{B.6}$$

where $I[\cdot]$ is the zero-ordered modified Bessel function of the first kind.

Then from Equation B.2 and Equation B.6, we get to our Equation 5.14.

REFERENCES

[1] R. L. Peterson, D. E. Borth and R. E. Ziemer, *An Introduction to Spread-Spectrum Communications*. 1995.

[2] C. E. Shannon, "Communication in the presence of noise," *Proceedings of the IRE*, vol. 37, no. 1, pp. 10-21, 1949.

[3] E. J. Candes, J. Romberg, and T. Tao, "Robust Uncertainty Principles: Exact Signal Reconstruction from Highly Incomplete Frequency Information," *IEEE Trans. on Information Theory*, vol. 52, no. 2, pp. 489-509, 2006.

[4] D. Donoho, "Compressed Sensing," *IEEE Trans. on Information Theory*, vol. 52, no. 4, pp. 1289-1306, 2006.

[5] E. J. Candes and J. Romberg, "Sparsity and Incoherence in Compressive Sampling," *Inverse Problems*, vol. 23, no. 3, pp. 969, 2007.

[6] D. Donoho, X. Huo, "Uncertainty principles and ideal atomic decomposition," *IEEE Trans. on Information Theory*, vol. 47, no. 7, pp. 2845-862, 2001.

[7] Bluetooth Special Interest Group, *https://www/bluetooth.org/Technical/Specifications/adopted.htm.*

[8] P. Kotowski and D. K., "Method of transmitting secret messages," Aug. 2 1940, uS Patent 2,211,132. [Online]. Available: http://www.google.com/patents/US2211132

[9] R. Scholtz, "The origins of spread-spectrum communications," *Communications, IEEE Transactions on*, vol. 30, no. 5, pp. 822–854, May 1982.

[10] "802.11-1999 - IEEE Standard for Information Technology- Telecommunications and Information Exchange Between Systems- Local and Metropolitan Area Networks- Specific Requirements- Part 11: Wireless LAN Medium Access Control (MAC) and Physical Layer (PHY) Specifications," *ANSI/IEEE Std 802.11, 1999 Edition (R2003)*, pp. 1-53, 2003

[11] "802.11b-1999 - Supplement to IEEE Standard for Information Technology-Telecommunications and Information Exchange Between Systems- Local and Metropolitan Area Networks- Specific Requirements- Part 11: Wireless LAN Medium Access Control (MAC) and Physical Layer (PHY) Specifications: Higher-Speed Physical Layer Extension in the 2.4 GHz Band," *IEEE Computer Society*, pp.1-90, 2000

[12] "802.11g-2003 - IEEE Standard for Information Technology- Telecommunications and Information Exchange Between Systems- Local and Metropolitan Area Networks- Specific Requirements Part Ii: Wireless LAN Medium Access Control (MAC) and Physical Layer (PHY) Specifications," *IEEE Computer Society*, pp. 1-67, 2003

[13] A. Mitra, "On Pseudo-Random and Orthogonal Binary Spreading Sequences," *International Journal of Information Technology, 2008*, vol. 4, no. 2, pp. 137-144, 2008.

[14] J. Lv and W. Qu, "Application of the Wavelet Rearrangement Algorithm in the Detection of Noncooperative Frequency Hopping Signals," *Signal Processing (ICSP), 2012 IEEE 11th International Conference on*, vol. 1, pp. 263-266, 2012.

[15] M. Sirotiya and A. Banerjee, "Detection and Estimation of Frequency Hopping Signals Using Wavelet Transform," *Cognitive Wireless Systems (UKIWCWS), 2010 Second UK-India-IDRC International Workshop on*, pp. 1-5, 2010.

[16] H. F. Overdyk, "Detection and Estimation of Frequency Hopping Signals Using Wavelet Transforms," *Monterey, California. Naval Postgraduate School*, 1997.

[17] K. Jaiswal, "Spectral Sensing for Cognitive Radio: Estimation of Adaptive Frequency Hopping Signal," *TENCON 2008 - 2008 IEEE Region 10 Conference*, pp. 1-5, 2008.

[18] K. Jaiswal, "Spectral Sensing of Adaptive Frequency Hopping signal for Cognitive Radio," *Performance, Computing and Communications Conference, 2008. IPCCC 2008. IEEE International*, pp. 360-365, 2008.

[19] M. P. Fargues, H. F. Overdyk, and R. Hippenstiel, "Wavelet-based Detection of Frequency Hopping Signals," *Signals, Systems amp; Computers, 1997. Conference Record of the Thirty-First Asilomar Conference on*, vol. 1, pp. 515-519, 1997.

[20] C. -D. Chung, "Generalised Likelihood-ratio Detection of Multiple-hop Frequency-hopping Signals," *Communications, IEE Proceedings-*, vol. 141, no. 2, pp. 70-78, 1994.

[21] C. -D. Chung, "Generalized Likelihood-ratio Detection of Multiple-hop Frequency-hopping Signals," *Military Communications Conference, 1991. MILCOM '91, Conference Record, Military Communications in a Changing World., IEEE*, vol. 2, pp. 527-531, 1991.

[22] R. A. Dillard and G. M. Dillard, "Likelihood-ratio Detection of Frequency-hopped Signals," *Aerospace and Electronic Systems, IEEE Transactions on*, vol. 32, no. 2, pp. 543-553, 1996.

[23] B. K. Levitt, U. Cheng, A. Polydoros and M. K. Simon, "Optimum Detection of Slow Frequency-hopped Signals," *Communications, IEEE Transactions on*, vol. 42, no. 234, pp. 1990-2000, 1994.

[24] B. Levitt, M. Simon, A. Polydoros, and U. Cheng, "Partial-band Detection of Frequency-hopped Signals," *Global Telecommunications Conference, 1993, including a Communications Theory Mini-Conference. Technical Program Conference Record, IEEE in Houston. GLOBECOM '93., IEEE*, vol. 4, pp. 70-76, 1993.

[25] W. E. Snelling and E. Geraniotis, "Sequential Detection of Unknown Frequency-hopped Waveforms," *Selected Areas in Communications, IEEE Journal on*, vol. 7, no. 4, pp. 602-617, 1989.

[26] H. Luan and H. Jiang, "Blind Detection of Frequency Hopping Signal Using Time-Frequency Analysis," *Wireless Communications Networking and Mobile Computing (WiCOM), 2010 6th International Conference on*, pp. 1-4, 2010.

[27] S. Luo and L. Luo, "Adaptive Detection of an Unknown FH Signal Based on Image Features," *Wireless Communications, Networking and Mobile Computing, 2009. WiCom '09. 5th International Conference on*, pp. 1-4, 2009.

[28] S. Luo and L. Luo, "Detection of an Unknown Frequency Hopping Signal Based on Image Features," *Image and Signal Processing, 2009. CISP '09. 2nd International Congress on*, pp. 1-4, 2009.

[29] J. Weber, K. Kowalske, C. Robertson, F. Kragh and C. Brown, "Detection of Frequency-Hopped Waveforms Embedded in Interference Waveforms with Noise," *Communications, 2007. ICC '07. IEEE International Conference on*, pp. 2973-2978, 2007.

[30] F. Javed and A. Mahmood, "The Use of Time Frequency Analysis for Spectrum Sensing in Cognitive Radios," *Signal Processing and Communication Systems (ICSPCS), 2010 4th International Conference on*, pp. 1-7, 2010.

[31] J. Hampton and John Oetting, "A Frequency Hopping Sequential Detection Technique for In-net Coarse Acquisition," *Military Communications Conference, 1992. MILCOM '92, Conference Record. Communications - Fusing Command, Control and Intelligence., IEEE*, vol. 1, pp. 43-47, 1992.

[32] H. Fan, Y. Guo and Y. Xu, "A Novel Algorithm of Blind Detection of Frequency Hopping Signal Based on Second-Order Cyclostationarity," *Image and Signal Processing, 2008. CISP '08. Congress on*, vol. 5, pp. 399-402, 2008.

[33] A. Polydoros and Kai Woo, "LPI Detection of Frequency-Hopping Signals Using Autocorrelation Techniques," *Selected Areas in Communications, IEEE Journal on*, vol. 3, no. 5, pp. 714-726, 1985.

[34] F. Ahmed and S. A. Khan, "A framework for Computationally Efficient Detection of Frequency Hopped Signals in Non-cooperative Environment," *Software, Telecommunications and Computer Networks, 2008. SoftCOM 2008. 16th International Conference on*, pp. 248-252, 2008.

[35] L. W. Nemsick and E. Geraniotis, "Adaptive Multichannel Detection of Frequency-hopping Signals," *Communications, IEEE Transactions on*, vol. 40, no. 9, pp. 1502-1511, 1992.

[36] L. W. Nemsick and E. Geraniotis, "Detection of Frequency Hopping Signals via Adaptive Multichannel Radiometry," *Military Communications Conference, 1992. MILCOM '92, Conference Record. Communications - Fusing Command, Control and Intelligence., IEEE*, vol. 3, pp. 1215-1220, 1992.

[37] J. J. Lehtomäki and M. Juntti, "Detection of Frequency Hopping Signals Using A Sweeping Channelized Radiometer," *Signal processing*, vol. 85, no. 10, pp. 2030-2043, 2005.

[38] J. J. Lehtomaki, M. Juntti and H. Saarnisaari, "Detection of Frequency Hopping Signals with A Sweeping Channelized Radiometer," *Signals, Systems and Computers, 2004. Conference Record of the Thirty-Eighth Asilomar Conference on*, vol. 2, pp. 2178-2182, 2004.

[39] G. R. Cooper, "Detection of Frequency-Hop Signals," *Military Communications Conference - Communications-Computers: Teamed for the 90's, 1986. MILCOM 1986. IEEE*, vol. 1, pp. 10.2.1-10.2.5, 1996.

[40] R. A. Dillard, "Detection of Spread-Spectrum Signals," *Decision and Control including the 16th Symposium on Adaptive Processes and A Special Symposium on Fuzzy Set Theory and Applications, 1977 IEEE Conference on*, vol. 16, pp. 529-535, 1977.

[41] R. A. Dillard, "Detectability of Spread-Spectrum Signals," *Aerospace and Electronic Systems, IEEE Transactions on*, vol. AES-15, no. 4, pp. 526-537, 1979.

[42] L. E. Miller, J. S. Lee and D. J. Torrieri, "Frequency-Hopping Signal Detection Using Partial Band Coverage," *Aerospace and Electronic Systems, IEEE Transactions on*, vol. 29, no. 2, pp. 540-553, 1993.

[43] J. J. Lehtomaki, "Maximum Based Detection of Slow Frequency Hopping Signals," *Communications Letters, IEEE*, vol. 7, no. 5, pp. 201-203, 2003.

[44] J. Joo, J. Won, C. Lee, S. Park and K. Lee, "Detection of an Unknown FH Signal Using Scanning Receiver and DF Receiver in Practical Environments," *Wireless Communications and Networking Conference, 2007.WCNC 2007. IEEE*, pp. 1226-1230, 2007.

[45] M. Song and S. Wigginton, "Frequency Hopping Pattern Detection in Wireless AD HOC Networks," *Information Technology: Coding and Computing, 2005. ITCC 2005. International Conference on*, vol. 2, pp. 633-638, 2005.

[46] M. A. Neifeld, A. Ashok and P. K. Baheti, "Task-specific information for imaging system analysis," *JOSA A, Optical Society of America*, vol. 24, no. 12, pp. B25-B41, 2007.

[47] H. Kim and N. A. Goodman, "Waveform design by Task-Specific Information," *Radar Conference, 2010 IEEE*, pp. 848-852, 2010.

[48] E. Arias-Castro and Y. C. Eldar, "Noise Folding in Compressed Sensing," *Signal Processing Letters, IEEE*, vol.18, no. 8, pp. 478-481, 2011.

[49] E. Adams, M. Gouda, and P. C. J. Hill, "Statistical techniques for blind detection discrimination of m-sequence codes in dsss systems," in *Proc. IEEE-ISSSTA*, 1998, p. 853857.

[50] J. D. Vlok, "Weak Signal (DSSS) Detection," *CSIR Little AOC Conference*, 2012.

[51] C. Bouder and G. Burel, "Spread spectrum codes identification by neural network," in *Systems and Control: Theory and Applications*, N. Mastorakis, Ed. WSES Press, 2000, pp. 257–262.

[52] J. D. Vlok, "Non-Cooperative Detection of Weak Spread-Spectrum Signals in Additive White Gaussian Noise," *Communications, IET*, vol. 6, no. 16, 2012

[53] H. Urkowitz, "Energy Detection of Unknown Deterministic Signal," *Proceedings of the IEEE*, vol. 55, no. 4, 1967

[54] Y. Lu and A. Finger, "Novel Multi-Correlation Differential Detection for Improving Detection Performance in DSSS," *Spread Spectrum Techniques and Applications (ISITA), 2010 IEEE 11th International Symposium on*, pp. 120-124, 2010.

[55] Z. Dong and H. Hu, "The Detection, Symbol Period and Chip Width Estimation of DSSS Signals Based on Delay-Multiply, Correlation and Spectrum Analysis," *Engineering Letters*, vol. 15, no. 1, pp. 140-144, 2007

[56] Z. Deng, L. Shen, N. Bao, B. Su, J. Lin and D. Wang, "Autocorrelation Based Detection of DSSS Signal for Cognitive Radio System," *Wireless Communications and Signal Processing (WCSP), 2011 International Conference on*, pp. 1-5, 2011.

[57] L. Chang, F. Wang and Z. Wang, "Detection of DSSS Signal in Non-Cooperative Communications," *Communication Technology, 2006. ICCT '06. International Conference on*, pp. 1-4, 2006.

[58] J. F. Kuehls and E. Geraniotis, "Presence Detection of Binary-Phase-Shift-Keyed and Direct-Sequence Spread-Spectrum Signals Using a Prefilter-Delay-and-Multiply Device," *Selected Areas in Communications, IEEE Journal on*, vol. 8, no. 5, 1990.

[59] G. Burel, "Detection of Spread Spectrum Transmissions Using Fluctuations of Correlation Estimators," *IEEE ISPACA*, 2000.

[60] G. Burel, C. Bouder and O. Berder, "Detection of Direct Sequence Spread Spectrum Transmissions without Prior Knowledge," *Global Telecommunications Conference, 2001. GLOBECOM '01. IEEE*, vol. 1, 2001.

[61] K. Fyhn, T. L. Jensen, T. Larsen and S. H. Jensen, "Compressive Sensing for Spread Spectrum Receivers," *Wireless Communications, IEEE Transactions on*, vol. 12, no. 5, pp. 2334-2343, 2013.

[62] T. Yucek and H. Arslan, "A Survey of Spectrum Sensing Algorithms for Cognitive Radio Applications," *Communications Surveys Tutorials, IEEE*, vol. 11, no. 1, pp. 116-130, 2009.

[63] S. S. Gishkori, *Compressive Sampling for PPM and FSK Modulated Signals*. Masters thesis, Delft University of Technology, 2009.

[64] Y. L. Polo, Y. Wang, A. Pandharipande and G. Leus, "Compressive Wide-band Spectrum Sensing," *Acoustics, Speech and Signal Processing, 2009. ICASSP 2009. IEEE International Conference on*, pp. 2337-2340, 2009.

[65] D. Yang, H. Li and G. D. Peterson, "Decentralized Turbo Bayesian Compressed Sensing with Application to UWB Systems," *EURASIP J. Adv. Sig. Proc.*, vol. 2011, 2011.

[66] Y. Wang, A. Pandharipande, Y. L. Polo and G. Leus, "Distributed Compressive Wide-band Spectrum Sensing," *Information Theory and Applications Workshop, 2009, IEEE*, pp. 178-183, 2009.

[67] J. A. Carreon and S. D. Cabrera, "Towards the Use of Learned Dictionaries and Compressive Sensing in Wideband Signal Detection," *SPIE Defense, Security, and Sensing, International Society for Optics and Photonics*, pp. 87170N-87170N, 2013.

[68] H. Sun, W. Chiu and A. Nallanathan, "Adaptive Compressive Spectrum Sensing for Wideband Cognitive Radios," *Communications Letters, IEEE*, vol. 16, no. 11, pp. 1812-1815, 2012.

[69] J. Laska, S. Kirolos, Y. Massoud, R. Baraniuk, A. Gilbert, M. Iwen and M. Strauss, "Random Sampling for Analog-to-Information Conversion of Wideband Signals," *Design, Applications, Integration and Software, 2006 IEEE Dallas/CAS Workshop on*, pp. 119-122, 2006.

[70] M. A. Davenport, Mi. B. Wakin and R. G. Baraniuk, "Detection and Estimation with Compressive Measurements," *Dept. of ECE, Rice University, Tech. Rep*, 2006.

[71] K. Fyhn, T. Arildsen, T. Larsen and S. H. Jensen, "Demodulating Subsampled Direct Sequence Spread Spectrum Signals Using Compressive Signal Processing," *Signal Processing Conference (EUSIPCO), 2012 Proceedings of the 20th European, IEEE*, pp. 2556-2560, 2012.

[72] J. Yuan, P. Tian and H. Yu, "Subspace Compressive Frequency Estimation of Frequency Hopping Signal," *Wireless Communications, Networking and Mobile Computing, 2009. WiCom '09. 5th International Conference on, IEEE*, pp. 1-4, 2009.

[73] J. Yuan, P. Tian and H. Yu, "The Detection of Frequency Hopping Signal Using Compressive Sensing," *Information Engineering and Computer Science, 2009. ICIECS 2009. International Conference on, IEEE*, pp. 1-4, 2009.

[74] J. Yuan, P. Tian and H. Yu, "The Identification of Frequency Hopping Signal Using Compressive Sensing," *Communications and Network, Scientific Research*, vol. 1, no. 1, pp. 52-56, 2009.

[75] M. A. Davenport, Mi. B. Wakin and R. G. Baraniuk, "The Compressive Matched Filter," *Tech. Rep. TREE 0610, Rice University*, 2006.

[76] M. K. Simon, S. M. Hinedi and W. C. Lindsey, *Digital Communication Techniques: Signal Design and Detection*. PTR Prentice Hall, sec. 5, 1994.

[77] R. O. Duda, P. E. Hart and D. G. Stork, *Pattern Classification*. Edition 2, Wiley, 2000.

[78] P. K. Baheti and M. A. Neifeld, "Adaptive Feature-specific Imaging: A Face Recognition Example," *Applied optics, Optical Society of America*, vol. 47, no. 10, pp. B21-B31, 2008.

[79] J. B. Kruskal, "Multidimensional Scaling by Optimizing Goodness of Fit to a Nonmetric Hypothesis," *Psychometrika*, vol. 29, no. 1, pp. 1-27, 1964.

[80] J. B. Kruskal and M. Wish, "Multidimensional Scaling," vol. 11, Sage, 1978.